AN ASTROBIOLOGICAL EXPLORATION OF MASS DEPENDENT AND MASS INDEPENDENT SULFUR ISOTOPE FRACTIONATION

UNEXPECTEDLY LARGE ISOTOPE FRACTIONATION DURING SULFIDE OXIDATION
LITHOLOGIC AND GEOLOGIC TEST OF THE MESOARCHAEAN S-MIF MINIMUM

Kristyn J. Rodzinyak

August 2012

Department of Earth and Planetary Sciences
McGill University
Montréal, Québec

A thesis submitted to the Faculty of Graduate Studies and Research in partial fulfillment of the requirements of the degree of Masters of Science

© K.J. Rodzinyak, 2012

Abstract

In this thesis, I examined multiple sulfur isotopes in two different systems: mass dependent fractionation and mass independent fractionation. Mass dependent sulfur isotopes elucidate low-temperature oxidative processes from pyrite nodules within Miocene lake sediments found in the Haughton impact structure on Devon Island, Nunuvat. Mass independent samples are investigated for lithological and geographical controls on the pattern of ^{33}S and ^{36}S anomalies in Mesoarchaean samples from Northwestern Ontario.

In mass dependent systems, the distribution of isotopes can be predicted based on the differences in mass of the various isotopes. Published studies of abiotic and biotic sulfur oxidation show negligible fractionation between starting sulfide and resulting sulfates. Pyrite nodules are being oxidized in a polar desert environment to a variety of sulfates including gypsum, jarosite, schwertmannite, and goethite. Within individual nodules, fractionation between sulfate and sulfide range from -10.1 to +17.9 ‰. In addition, a two-component mixing between pyrite and bedrock sulfates divides the nodules into three types. The first two are explained by conventional oxidation and mixing; however, most samples cannot be described solely through mixing or oxidation. Measuring large fractionations in sulfide oxidation has implications for the study of 'biosignatures' such that an oxidizing environment, for example the surface of Mars, would be incompatible with the preservation of 'biosignatures'.

In samples older than approximately 2.45 billion years, mass independent fractionation is observed in rock samples. These anomalous enrichments or depletions in ^{33}S cannot be predicted solely on mass differences; rather they are attributed to photochemical reactions of SO_2 in an oxygen poor atmosphere. Within the Mesoarchaean the magnitude of these anomalous ^{33}S measurements are considerably diminished compared to contiguous time periods. Previous work has focused on changes in atmospheric chemistry to explain these minimum values. By looking at samples from Northwestern Ontario, the effect of lithology and geography are tested. In addition, a sulfur isotope database compiles the literature data. The range of multiple sulfur isotope data is extended as compared to the data from South Africa and Australia; however, the magnitude remains small when compared to adjacent time periods. Nevertheless, the isotope systematics of the Mesoarchaean, with this added dataset, follow the Archaean reference array which has previously not been used for the Mesoarchaean samples. Regarding lithology, chemically and biologically precipitated samples show large variation in anomalous ^{33}S whereas clastic rocks remain close to zero.

Résumé

Cette étude se penche sur le comportement des différents isotopes du soufre dans deux systèmes distincts : le fractionnement dépendant de la masse et le fractionnement indépendant de la masse. Les isotopes du soufre dépendants de la masse élucident les procédés oxydants de basse température dans des nodules de pyrite de sédiments lacustres d'âge Miocène trouvés dans la structure d'impact Haughton sur l'Île Devon. Les échantillons indépendants de la masse ont été étudiés afin d'évaluer les contrôles lithologique et géographique sur les anomalies en ^{33}S et ^{36}S d'échantillons Mésoarchéens du nord-ouest de l'Ontario.

Pour les systèmes dépendants de la masse, la distribution des isotopes peut être prédite en fonction des différences de masse des isotopes. Les ouvrages publiés traitant de l'oxydation abiotique et biotique du soufre démontrent un fractionnement négligeable entre les sulfites d'origine et les sulfates résultants. Les nodules de pyrite ont été oxydées dans un environnement polaire désertique pour former différents sulfates, comme le gypse, la jarosite, la schwertmannite, et la goethite. À l'intérieur des nodules, le fractionnement entre sulfates et sulfites varie de -10.1 à +17.9 ‰. De plus, un mélange à deux composants entre la pyrite et les sulfates du substrat rocheux divise les nodules en trois types. Les deux premiers sont expliqués par des procédés d'oxydation et de mélange conventionnels, bien que la plupart des échantillons ne peuvent être décrits uniquement en termes de mélange ou d'oxydation. La mesure de grands fractionnements associés à l'oxydation des sulfites a des implications pour l'étude de « biosignatures » puisqu'un

environnement oxydant, par exemple la surface de Mars, serait incompatible avec la préservation de telles « biosignatures ».

Pour les échantillons rocheux vieux de plus de 2.45 milliards d'années, on observe le fractionnement indépendant de la masse. Ces augmentations ou réductions anormales en ^{33}S ne peuvent pas être expliquées seulement par la différence de masse. Celles-ci sont plutôt attribuées aux réactions photochimiques du SO_2 dans une atmosphère pauvre en oxygène. Au cours de Mésoarchéen l'ampleur de ces mesures anormales en ^{33}S sont considérablement diminuées en comparaison avec les périodes de temps adjacentes. Les travaux antérieurs se sont concentrés sur les changements de la chimie atmosphérique pour expliquer le minimum. En considérant des échantillons du nord-ouest ontarien, les effets lithologiques et géographiques sont testés. En plus, une base de données des isotopes du soufre compile les données de la littérature. La variation des données sur les multiples isotopes du soufre est étendue en rapport aux données du l'Afrique du Sud et de l'Australie. Par contre, l'amplitude du fractionnement demeure limitée en comparaison aux périodes adjacentes. Toutefois, la systématique isotopique du Mésoarchéen, avec ces données additionnelles, suit les valeurs de référence de l'Archéen alors que celles-ci n'avaient pas été utilisées jusqu'ici pour des échantillons Mésoarchéens. En ce qui concerne les effets lithologiques, les échantillons précipités lors de procédés chimiques et biologiques montrent de grandes variations en ^{33}S anormal alors que les roches clastiques demeurent près de la valeur zéro.

Acknowledgments

A very special thank you to everyone who has helped with the creation of this thesis. Principally to my advisors from whom I have learned so much over the past two years: Boz and Richard. Also to the PROPS group who make coming into school everyday so much fun and for their discussions and help with lab: André Pellerin, Thi Hao Bui, Grant Cox, Emma Bertran, Matt Hryciuk, John Prince, Clint Scott, Marcus Kunzman, and Lucie Hubert and my colleagues at the Canadian Space Agency: Richard Léveillé, Caroline-Emmanuelle Morisset, Pablo Sobron Sanchez, Jason Clement, Marilyn Steinberg and the many students. Merci Marc-Antoine for translating my abstract. Thank you to the EPS staff Anne, Kristy, Angela, and Brigitte for all their help and smiles.

To Phil Thurston, Andrey Bekker, Christie Rowe and Boz Wing for two wonderful field summers with great outcrop learning. To my fellow grad students from McGill working in the same area Nils Backeberg and Rob Borowski, thanks for adding such entertainment to the field season. Special thanks for the patience of my three great field assistants Aeron Vaillancourt, Ian Calvaho Campos and Léa Braschi. Léa also ran several sulfur isotope extractions for me. Logistics and outcrops were much easier to find with the assistance of the Red Lake District Geology Office. Thanks to Sam, Carmen Storey and Andreas Lichtblau for braving all sorts of weather. The Thunder Bay District Geology office and core shed especially to Dorothy Campbell. Sara Buse of the Ontario Geological Survey for great outcrop advice in the Lumby Lake area.

Additionally, thanks go out to Osisko at the Hammond Reef Project specifically Denver Stone for the field support. Financial support for the thesis was provided through an NSERC grant, the Canadian Astrobiology Training Program and the research affiliate program at the Canadian Space Agency.

Finally, to my amazing family Mom, Dad, Daphne, and Celina for the many phone calls, visits and putting up with my scientific babel I could not have done it without you.

KJR

Contribution of Authors

Unexpectedly large sulfur isotope fractionation during low temperature oxidation, Devon Island, Canada

Richard Léveillé collected the samples from Devon Island. Boswell Wing calculated $^{33}\lambda$ for the type 3 samples. Both co-authors provided much discussion and guidance regarding the direction of research and manuscript. Kristyn completed the sample preparation, chemical extractions, mass spectrometer results and the write-up.

Lithologic and geographic test of the Mesoarchaean S-MIF minimum

Boswell Wing contrived the concept for the project and organized the first field season. Support and guidance through all parts of the field, lab work and manuscript were incredibly valuable. Sample preparation, chemical extractions, mass spectrometer analyses and manuscript were completed as part of this MSc thesis.

Table of Contents

Manuscript 1: Unexpectedly large sulfur isotope fractionation during low temperature oxidation of pyrite, Devon Island, Canada

Manuscript 2: Lithologic and geographic test of the Mesoarchaean S-MIF minimum, Northwestern Ontario, Canada

List of figures, images, and tables

Introduction

Manuscript 1:

Unexpectedly large sulfur isotope fractionation during low temperature oxidation of pyrite, Devon Island, Canada

Manuscript 2:

Lithologic and geographic test of the Mesoarchaean S-MIF minimum

Introduction

Sulfur is an important element for many earth system processes. It is polyvalent and is the 10th most abundant element in the universe (Seal II, 2006). There are four stable isotopes of sulfur: ^{32}S, ^{33}S, ^{34}S, and ^{36}S, with terrestrial abundances of 94.93%, 0.76%, 4.29%, and 0.02% respectively (Coplen et al., 2002). Because of the sensitivity of sulfur isotopes to sulfur sources and mechanisms of sulfur cycling, sulfur isotope ratios can be used to constrain important geological and biological processes. The applications of sulfur isotopes are quite varied and range from the biological sulfur cycle, to volcanic gases and composition of the ocean, to sulfide-bearing economic mineralization, as well as to evolution of life (Thode, 1991). In this thesis I apply multiple sulfur isotope analyses to two different systems that illustrate this potential.

Sulfur isotope systematics: Sulfur isotope compositions are expressed using delta notation. The delta notation relates the relative ratio of the isotope of interest to the most abundant isotope (^{32}S) compared to that ratio in a standard.

$$\delta^{M}S = \left[\frac{\left({}^{M}S/{}^{32}S\right)_{sample}}{\left({}^{M}S/{}^{32}S\right)_{standard}} - 1\right] \times 1000\ [‰]$$

M is 33, 34 or 36. The standard used for sulfur isotope measurements is the Vienna Cañon Diablo Troilite (V-CDT), which approximates the bulk sulfur isotopic composition of meteoritical sulfur, and is defined by the sulfur isotope content in the international reference Ag_2S IAEA-S-1. IAEA-S-1 has a $\delta^{34}S$ value of -0.3‰. In this thesis I consider the $\delta^{33}S$ value to be -0.061 ‰, and the $\delta^{36}S$ value to be -1.27‰

Isotopes are generally distributed between two sulfur-bearing compounds based on mass differences. Within the sulfur system, the mass difference between ^{32}S and ^{33}S is approximately 1 atomic mass unit (amu), compared to ^{34}S and ^{32}S with a mass difference of approximately 2 amu. These mass differences yield a slope of approximately 0.5 when comparing $\delta^{33}S$ values to $\delta^{34}S$ values as shown in Figure 1. Isotopic measurements that follow this relationship are known as mass dependent, and together define the terrestrial fractionation line for sulfur isotopes. Mass dependent relationships, however, are also present in meteorites (Hulston and Thode, 1965). The terrestrial fractionation line reflects the isotopic consequences of processes like sulfate reduction by bacteria, volcanic degassing, and mineral-fluid interaction. All of these mass-dependent processes are affected by some general isotopic principles as outlined below.

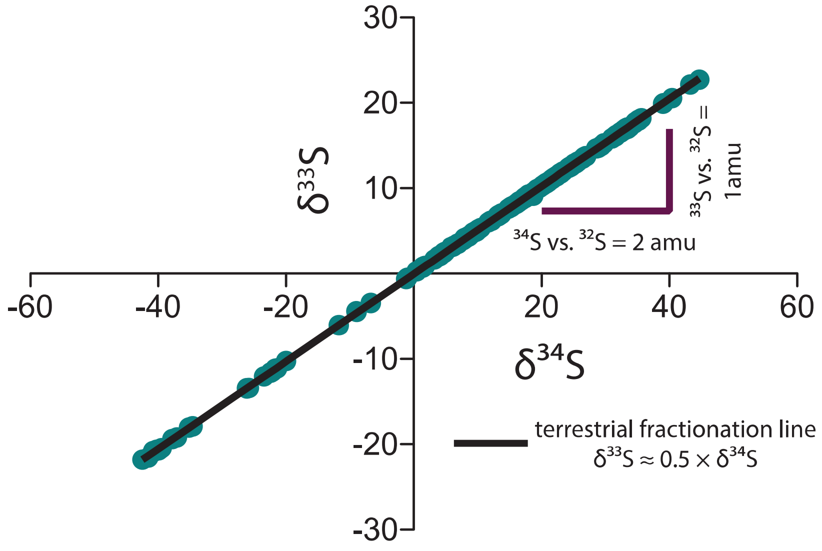

Figure I: $\delta^{33}S$ versus $\delta^{34}S$ measurements for terrestrial sulfides younger than ~2.45 Ga. The sulfur isotopes follow mass dependent relationships and fall along the terrestrial fractionation line. Data from (Domagal-Goldman et al., 2008; Farquhar et al., 2000; Hu et al., 2003; Johnston et al., 2008; Johnston et al., 2006; Johnston et al., 2005; Rouxel et al., 2008).

General principles of isotope fractionation: Equilibrium isotope fractionation involves completely reversible reactions between two sulfur-bearing compounds such that there is no net change in the abundance of one or the other. On the other hand, kinetic isotope fractionation involves net unidirectional processes, where a sulfur-bearing compound is produced at the expense of a sulfur-bearing reactant. While the magnitude of a kinetic isotope fractionation can be affected by reaction rate, reaction pathway and whether product is continuously lost (open system) or lost entirely at once (closed system), both equilibrium and kinetic isotope fractionations are fundamentally controlled by variations in bond stabilities of isotopically substituted molecules.

Chemical bonds involving the heavier isotope (^{34}S) tend to have lower vibrational frequencies and, as a result, zero-point energies that are nearer to the minimum energy of the potential energy surface for a given bond. Accordingly, in a system of two isotopes (^{34}S and ^{32}S) and two distinct sites available for sulfur bonds, the energy of the system will be minimized if the heavier isotope is partitioned into the site with the stronger bond. This conceptually describes the origin of equilibrium isotope effects. Bonds with lower vibrational frequencies, and lower zero-point energies, will require more energy for the bonded atoms to leave the potential energy well and break the bond. Since heavy isotopes make stronger bonds, which are harder to break, bonds in a reactant molecule that contain light isotopes will react faster, causing products to become enriched in the lighter isotope. This conceptually describes kinetic isotope effects and how chemical reactions result in the partitioning of isotopes. The enrichment of the light isotope (e.g., ^{32}S) in the product species is called a normal isotope effect (Sharp, 2007).

Studies of sulfur isotope fractionation: The study of equilibrium and kinetic sulfur isotope fractionation began in the 1940s (Thode et al., 1949; Trofimov, 1949). Early on it was recognized that sulfate species tend to be enriched in the heavier isotopes compared to sulfide species (Thode et al., 1949), as would be expected from theoretical predictions of equilibrium sulfur isotope fractionation (Thode, 1991). However, the most important factor determining whether equilibrium is attained during of sulfur isotope exchange between oxidized (sulfate) and reduced (sulfide) species is pH, with temperature also playing a role (Ohmoto and Lasaga, 1982). Equilibrium between sulfide and sulfate species generally only occurs at high temperatures (200-400°C) and low pH (<3) (Rye, 2005).

In contrast, large sulfur isotope fractionations are associated with the metabolic byproducts of sulfate reducing bacteria, even at low temperatures (Canfield, 2001; Kaplan and Rittenberg, 1964). For example, fractionations up to 66‰ ($\delta^{34}S_{sulfate} - \delta^{34}S_{sulfide}$) are reported for the marine bacterial *Desulfovibrio* (Sim et al., 2011). In nature, even higher fractionations of 72‰ are reported for *in-situ* sulfate reduction in an Australia sediment core with hypersulfidic interstitial waters (Wortmann et al., 2001).

Maximum sulfur isotope fractionations correspond to the summation of the isotope effects of the individual steps in sulfate reduction (Canfield, 2001) such as in the steady state model of Rees (Rees, 1973). Brunner and Bernasconi (2005) reevaluated the Rees model postulating that large fractionations accompanying sulfate reduction could result from a high degree of reversibility associated with low energy supply in high sulfide conditions (Brunner and Bernasconi, 2005). Alternatively, large depletions in ^{34}S in sulfide relative to sulfate may represent the re-oxidation of sulfur in the sulfide species, and the subsequent disproportionation of the re-oxidized sulfur to sulfate and sulfide (Canfield and Thamdrup, 1994). A critical assumption in this model is that sulfur isotope fractionation during the oxidation of sulfide is minimal. This assumption has been verified in experiments, where biotic and abiotic sulfur oxidation generally produces small inverse isotope effects (Fry et al., 1984; Fry et al., 1988).

There are exceptions to the tendency of isotopes to fractionate in a mass dependent manner. In the 1960s, Hulston and Thode postulated that deviations from mass dependent fractionation would be a result of nuclear as opposed to chemical or physical processes (Hulston and Thode, 1965). Measurements of sulfur isotopes in meteorites led to the recognition of the presence of mass independent processes in the early solar nebula (Thiemens, 1999). In contrast, mass independent sulfur isotope fractionation (S-MIF) in terrestrial samples has been interpreted as being produced by photolysis of volcanic SO_2 in the atmosphere in a low oxygen environment (Farquhar et al., 2000). Photochemical experiments indicate that non-mass dependent behavior can occur during low-oxygen reactions with ultraviolet light and sulfur dioxide. (Danielache et al., 2008; Farquhar et al., 2001; Lyons, 2007; Pen and Clayton, 2008; Wing et al., 2004). Deviations from the mass dependent terrestrial fractionation line for sulfur isotopes are described using capital delta notation (Δ) as illustrated in figure II.

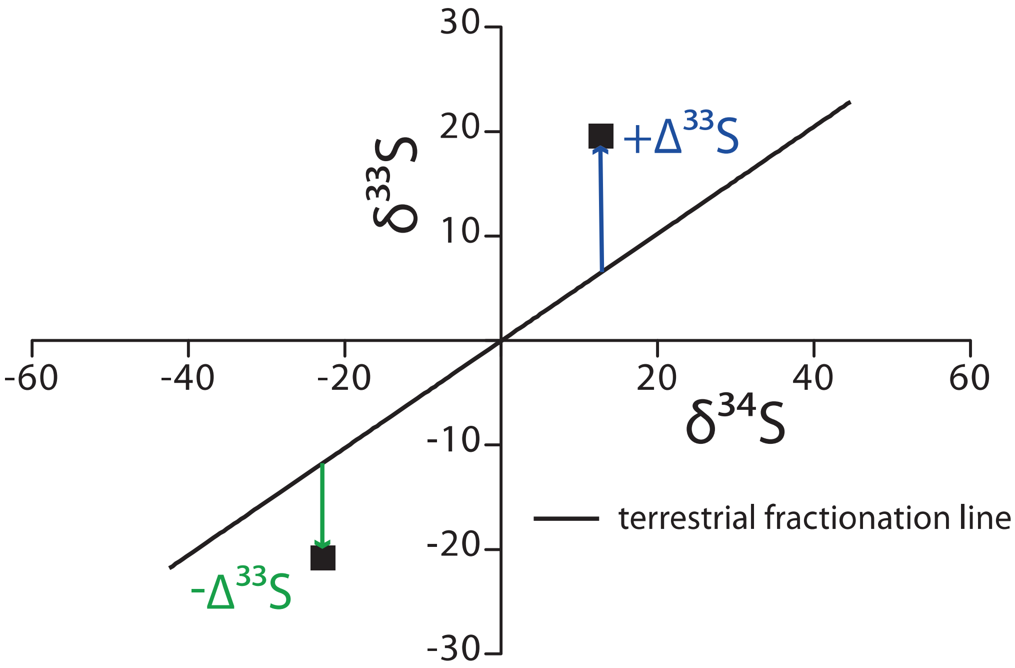

Figure II: Mass independent fractionation causes isotopic measurements to plot off the predicted mass dependent slope. If samples are below the terrestrial fractionation line they are –Δ^{33}S if they are above the slope they are +Δ^{33}S.

There is a binary structure to the record of terrestrial Δ^{33}S values versus time as illustrated in figure III. Post ~2.45 Ga samples have no anomalous enrichment or depletion in ^{33}S while pre ~2.45 Ga samples show large enrichments and depletion in ^{33}S. This binary structure has been used as a "smoking gun" proxy for a step change in atmospheric oxygen levels at 2.45 Ga as anomalous sulfur isotope enrichments and depletions are interpreted to form while atmospheric oxygen is low.

Additionally there are finer scale variations within the Archaean samples. A primary example is the period of small magnitude Δ^{33}S values around 3.0 Ga, known as the Mesoarchaean minimum. There have been a variety of complex atmospheric models to explain this Mesoarchaean minimum. These include a whiff of oxygen preceding the Great Oxygenation Event at 2.45 Ga, methane haze, and a change in the style of volcanism (Domagal-Goldman et al., 2008; Farquhar et al., 2007; Halevy et al., 2010; Ohmoto et al., 2006). Increased oxygen would limit both S-MIF production and preservation. A methane haze would block some of the UV that are necessary for the photodissociation reaction (Domagal-Goldman et al., 2008), potentially causing smaller magnitude S-MIF in the geological record. The ratio of SO_2:H_2S in volcanic gases is a function of volcanic environment, and lower ratios would presumably cause less S-MIF as H_2S does not undergo mass-independent fractionation during atmospheric photolysis. The transition out of the Mesoarchaean minimum may record a transition from predominately submarine volcanism to more subaerial volcanism, which may increase the SO_2:H_2S ratio in volcanic gases (Halevy et al., 2010).

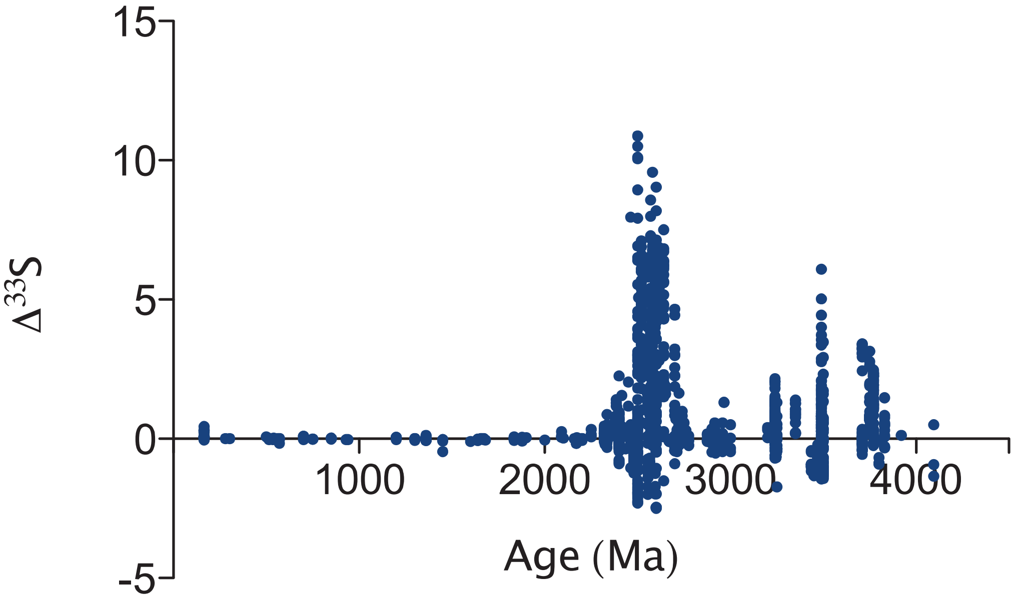

Figure III: Compilation of published $\Delta^{33}S$ values over time.

The purpose of this thesis is two fold. The two projects look at different systems using the same tool – multiple sulfur isotopes. The first chapter uses mass independent fractionation in sulfur isotopes to address the issue of the Mesoarchaean minimum. The second chapter looks at mass dependent fractionation of sulfur isotopes to evaluate the canonical idea that sulfur oxidation cannot cause significant isotopic fractionation.

In the first chapter, prior to invoking any complex atmospheric models to address the Mesoarchaean minimum, I aim to investigate whether the pattern reflects a sampling bias. Samples for the Mesoarchaean minimum are dominantly from South Africa with some limited samples from Australia, potentially leading to a geographic bias in the record. Additionally, the link between lithology and the preserved $\Delta^{33}S$ values has not been thoroughly investigated. Many of the Mesoarchaean samples are shales but most are listed by formation rather a specific lithology. This first chapter aims to evaluate the effects of both the geographic and lithologic distribution of the Mesoarchaean sulfur isotope record. Our study area of Northwestern Ontario allows us to test another sample location. In addition, a multitude of lithologies from each sampling area are investigated to evaluate the influence of lithology on the MIF signal.

In the second chapter, multiple sulfur isotopes are applied to evaluate the current paradigm for sulfur oxidation, which stipulates that no fractionation occurs between the parent sulfide and the resulting sulfate products. In this chapter the study area is Devon Island in the Canadian Arctic where the Haughton Impact Structure was subsequently filled with lake sediments. These lake sediments, in at least one locality, host pyrite nodules that are being oxidized to a variety of sulfates including jarosite, schwertmannite, and gypsum. I used multiple sulfur isotopes to learn more about the processes involved in these nodules including sulfide oxidation and sulfate alteration mineral formation.

Works Cited

Brunner, B. and Bernasconi, S. M., 2005. A revised isotope fractionation model for dissimilatory sulfate reduction in sulfate reducing bacteria. *Geochimica Et Cosmochimica Acta* **69**, 4759-4771.

Canfield, D. E., 2001. Biogeochemistry of sulfur isotopes, *Stable Isotope Geochemistry*.

Canfield, D. E. and Thamdrup, B., 1994. The production of S-34 depleted sulfide during bacterial disproportionation of elemental sulfur. *Science* **266**, 1973-1975.

Coplen, T., Bohlke, J., De Bievre, P., Ding, T., Holden, N., Hopple, J., Krouse, H., Lamberty, A., Peiser, H., Revesz, K., Rieder, S., Rosman, K., Roth, E., Taylor, P., Vocke, R., and Xiao, Y., 2002. Isotope-abundance variations of selected elements (IUPAC Technical Report). *Pure and Applied Chemistry* **74**, 1987-2017.

Danielache, S. O., Eskebjerg, C., Johnson, M. S., Ueno, Y., and Yoshida, N., 2008. High-precision spectroscopy of S-32, S-33, and S-34 sulfur dioxide: Ultraviolet absorption cross sections and isotope effects. *Journal of Geophysical Research-Atmospheres* **113**.

Domagal-Goldman, S. D., Kasting, J. F., Johnston, D. T., and Farquhar, J., 2008. Organic haze, glaciations and multiple sulfur isotopes in the Mid-Archean Era. *Earth and Planetary Science Letters* **269**, 29-40.

Farquhar, J., Bao, H. M., and Thiemens, M., 2000. Atmospheric influence of Earth's earliest sulfur cycle. *Science* **289**, 756-758.

Farquhar, J., Peters, M., Johnston, D. T., Strauss, H., Masterson, A., Wiechert, U., and Kaufman, A. J., 2007. Isotopic evidence for Mesoarchaean anoxia and changing atmospheric sulphur chemistry. *Nature* **449**, 706-709.

Farquhar, J., Savarino, J., Airieau, S., and Thiemens, M. H., 2001. Observation of wavelength-sensitive mass-independent sulfur isotope effects during SO2 photolysis: Implications for the early atmosphere. *Journal of Geophysical Research-Planets* **106**, 32829-32839.

Fry, B., Gest, H., and Hayes, J. M., 1984. Isotope effects associated with the anaerobic oxidation of sulfide by the purple photosynthetic bacterium, Chromotium vinosum. *Fems Microbiology Letters* **22**, 283-287.

Fry, B., Ruf, W., Gest, H., and Hayes, J., 1988. Sulfur isotope effects associated with oxidation of sulfide by O2 in aqueous solution. *Chemical Geology* **73**, 205-210.

Halevy, I., Johnston, D. T., and Schrag, D. P., 2010. Explaining the Structure of the Archean Mass-Independent Sulfur Isotope Record. *Science* **329**, 204-207.

Hu, G., Rumble, D., and Wang, P., 2003. An ultraviolet laser microprobe for the in situ analysis of multisulfur isotopes and its use in measuring Archean sulfur isotope mass-independent anomalies. *Geochimica Et Cosmochimica Acta* **67**, 3101-3118.

Hulston, J. R. and Thode, H. G., 1965. Variations in S33 S34 and S36 contents of meteorites and their relation to chemical and nuclear effects. *Journal of Geophysical Research* **70**, 3475-3484.

Johnston, D. T., Farquhar, J., Summons, R. E., Shen, Y., Kaufman, A. J., Masterson, A. L., and Canfield, D. E., 2008. Sulfur isotope biogeochemistry of the Proterozoic McArthur Basin. *Geochimica Et Cosmochimica Acta* **72**, 4278-4290.

Johnston, D. T., Poulton, S. W., Fralick, P. W., Wing, B. A., Canfield, D. E., and Farquhar, J., 2006. Evolution of the oceanic sulfur cycle at the end of the Paleoproterozoic. *Geochimica Et Cosmochimica Acta* **70**, 5723-5739.

Johnston, D. T., Wing, B. A., Farquhar, J., Kaufman, A. J., Strauss, H., Lyons, T. W., Kah, L. C., and Canfield, D. E., 2005. Active microbial sulfur disproportionation in the Mesoproterozoic. *Science* **310**, 1477-1479.

Kaplan, I. R. and Rittenberg, S. C., 1964. Microbiological fractionation of sulphur isotopes. *Journal of General Microbiology* **34**, 195-212.

Lyons, J. R., 2007. Mass-independent fractionation of sulfur isotopes by isotope-selective photodissociation of SO2. *Geophysical Research Letters* **34**.

Ohmoto, H. and Lasaga, A., 1982. Kinetics of reactions between aqueous sulfates and sulfides in hydrothermal systems. *Geochimica Et Cosmochimica Acta* **46**, 1727-1745.

Ohmoto, H., Watanabe, Y., Ikemi, H., Poulson, S. R., and Taylor, B. E., 2006. Sulphur isotope evidence for an oxic Archaean atmosphere. *Nature* **442**, 908-911.

Pen, A. and Clayton, R. N., 2008. Non-mass dependent fractionation of sulfur and oxygen isotopes during SO_2 UV photolysis*American Geophysical Union, Fall Meeting*, San Francisco.

Rees, C. E., 1973. Steady-state model for sulfur isotope fractionationin bacterial reduction processes. *Geochimica Et Cosmochimica Acta* **37**, 1141-1162.

Rouxel, O., Ono, S. H., Alt, J., Rumble, D., and Ludden, J., 2008. Sulfur isotope evidence for microbial sulfate reduction in altered oceanic basalts at ODP Site 801. *Earth and Planetary Science Letters* **268**, 110-123.

Rye, R., 2005. A review of the stable-isotope geochemistry of sulfate minerals in selected igneous environments and related hydrothermal systems. *Chemical Geology* **215**, 5-36.

Seal II, R. R., 2006. Sulfur Isotope Geochemistry of Sulfide Minerals. Reviews in Mineralogy and Geochemistry.

Sharp, Z., 2007. *Principles of stable isotope geochemistry*. Pearson Prentice Hall, Upper Saddle River, NJ.

Sim, M., Bosak, T., and Ono, S., 2011. Large Sulfur Isotope Fractionation Does Not Require Disproportionation. *Science* **333**, 74-77.

Thiemens, M. H., 1999. Atmosphere science - Mass-independent isotope effects in planetary atmospheres and the early solar system. *Science* **283**, 341-345.

Thode, H., 1991. Sulfur Isotopes in Nature and the Environment: An Overview. In: Krouse, H. and Grinkenko, V. Eds.), *Stable Isotopes: Natural and Anthropogenic Sulphur in the Environment*. John Wiley & Sons, Chicester, New York, Brisbane, Toronto, Singapore.

Thode, H., MacNamara, J., and Collins, C., 1949. Natural variations in the isotopic content of sulphur and their significance. *Canadian Journal of Research Section B-Chemical Sciences* **27**, 361-373.

Trofimov, A., 1949. Isotopic composition of sulfur in meteorites and terrestrial objects. *Daklady Akad. Nauk SSSR* **66**, 181-4.

Wing, B. A., Lyons, J. R., and Farquhar, J., 2004. Experimental SO_2 photochemistry and anomalous S isotope fractionation. *228th ACS National Meeting*, Philadelphia, PA.

Wortmann, U. G., Bernasconi, S. M., and Bottcher, M. E., 2001. Hypersulfidic deep biosphere indicates extreme sulfur isotope fractionation during single-step microbial sulfate reduction. *Geology* **29**, 647-650.

Unexpectedly large sulfur isotope fractionation during low temperature oxidation of pyrite, Devon Island, Canada

K.J. Rodzinyak., B.A. Wing, R.J. Léveillé

Introduction

Current models for sulfide oxidation acknowledge sulfur isotope consistency between parent sulfide and oxidative products (Seal II, 2006). Previous research suggests that the sulfur isotope composition of parent sulfides should be similar to their oxidative products (Balci et al., 2007; Brabec et al., 2012; Seal II, 2006). In this way, sulfide oxidation is quite distinct from sulfate reduction, which has large fractionation values ($\delta^{34}S_{sulfate}$ -$\delta^{34}S_{sulfide}$ up to ≈70‰) as reported for prokaryotic sulfate reduction (Canfield, 2001; Chambers and Trudinger, 1978; Kaplan and Rittenberg, 1964; Sim et al., 2011; Thode, 1991).

Previous abiotic and biological studies report small normal or inverse isotope effects for sulfur oxidation. The fractionation values range from approximately -5 to +3 ‰ but most studies showed that this was negligible (Fry et al., 1986; Fry et al., 1984; Fry et al., 1988; Taylor et al., 1984a, b; Toran and Harris, 1989; Zerkle et al., 2009). One study found a surprisingly large fractionation value of -18 ‰ for sulfate relative to the starting sulfide for *Thiobacillus concretivorus*; this was attributed to the formation of intermediaries like polythionates (Kaplan and Rittenberg, 1964). However, this large fractionation has not be replicated in the literature (Fry et al., 1986; Thode, 1991).

In this study, sulfur oxidation in a cold dry environment was examined using multiple sulfur isotopes. We studied the sulfur isotope systematics of mineralized sulfate-bearing crusts on sedimentary pyrite nodules from Devon Island in the Canadian Arctic. These pyrite nodules oxidize in a polar desert environment to form alteration products including a variety of sulfates.

Geological Setting

Devon Island, Nunavut, is the fourth largest island in the Canadian Arctic Archipelago. The Haughton Impact structure [39 ± 2 Ma] (Sherlock et al., 2005) is located on the island. The Paleozoic sedimentary package hosting the Haughton Impact structure contains thick sequences of carbonates and Ordovician sulfate evaporites, which gave rise to the predominantly carbonate- and sulfate-rich melt rocks within the crater (Osinski and Spray, 2003). Lacustrine sediments were deposited in the crater during the Miocene epoch (Hickey et al., 1988; Osinski et al., 2005c). Presently 9 km^2 of the resulting Haughton Formation (Figure 1.2) are exposed on the surface, and consist of dolomitic silt and mud with some fine sand (Mayr, 1987; Osinski and Lee, 2005b). At rare locations (Figure 1.1) within the dolomitic silt of the Haughton Formation there are pyrite nodules ranging from several cm up to 10s of cm across (Figure 1.3). The mineralogy of these nodules includes pyrite, gypsum, goethite, schwertmannite and jarosite (Léveillé, 2007).

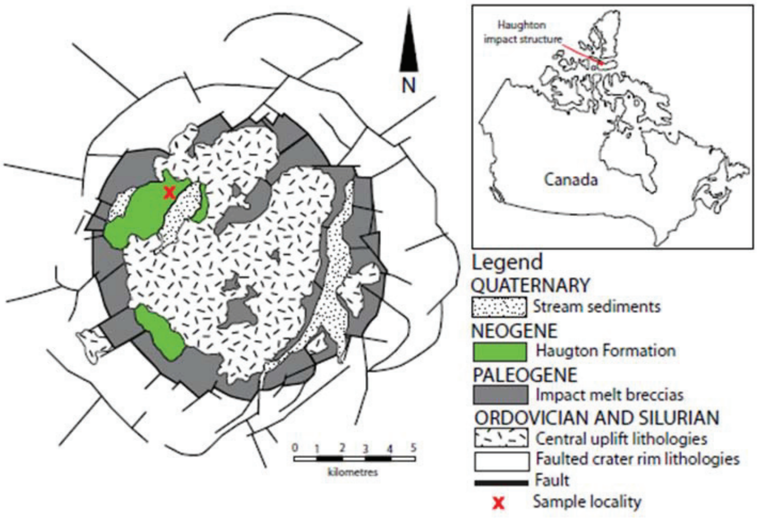

Figure 1.1: Simplified geological map of the Haughton impact structure located on Devon Island in the Canadian arctic. After (Osinski et al., 2005a; Sherlock et al., 2005)

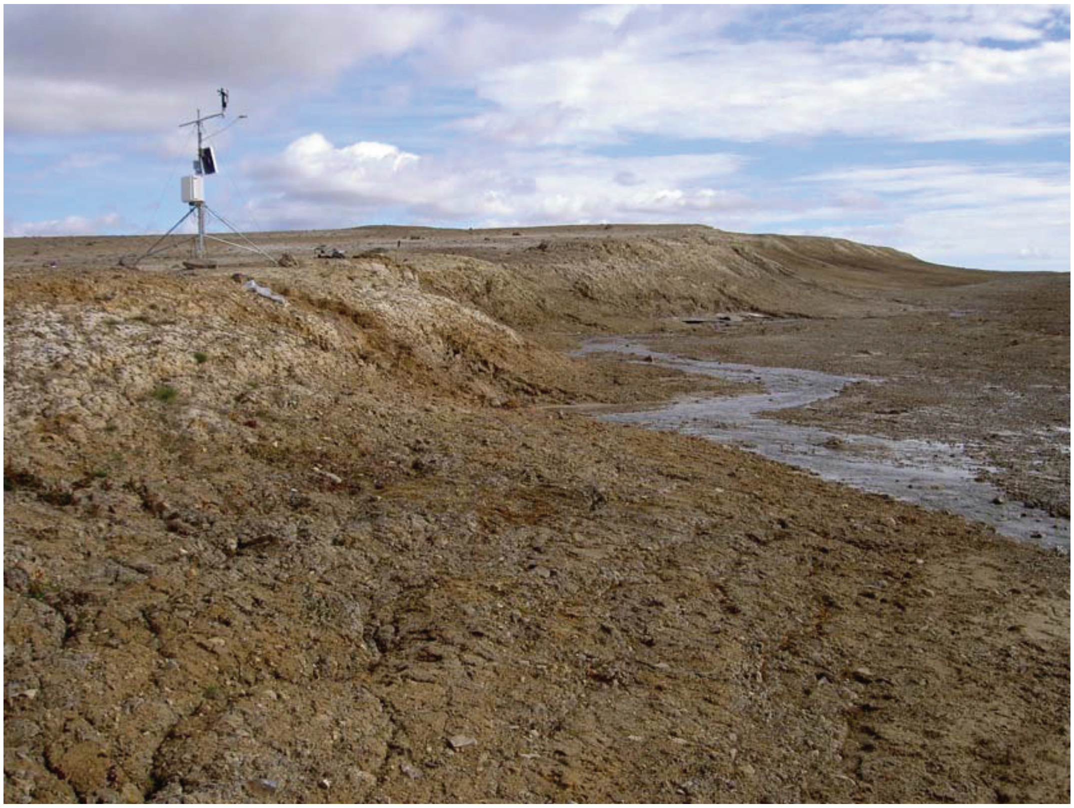

Figure 1.2 : Sampling location on Devon Island. The host rocks are Miocene lake sediments of the Haughton Formation within the Haughton impact structure. Devon Island is a polar desert with average temperatures of -17°C. For scale, the weather station is ~ 3 m.

Figure 1.3 : Nodules in situ in dolomitic silt. Orange discolouration shows location of the oxidized pyrite nodules. Surrounding grey are dolomitic silts of the Haughton Formation. Pen for scale is ~14 cm.

Methods

We collected nodules of varying degrees of oxidation from the dolomitic silts of the Haughton Formation. Some samples were collected from the surface while others were dug out from the unconsolidated silt. Less oxidized nodules are grey to black. The mineralogy of these nodules is primarily pyrite with a minor coating of gypsum. More oxidized nodules are less competent, reddish orange, and dusted with a coating of yellow powder (Figure 1.4). Powder X-ray diffraction shows that they consist primarily of gypsum, goethite and jarosite-group minerals. Sodium, potassium and hydronium jarosite are all present but these minerals rarely occur in samples with pyrite present (Léveillé, 2007).

Bulk sulfide and sulfate were chemically extracted from each of the twelve powdered nodules, which ranged in mineral composition from predominately pyrite to predominantly sulfate with no pyrite. Sulfides were extracted using chromium reducing solution while sulfates were extracted with Thode reagent (Fossing and Jorgensen, 1989). First all sulfides were removed by using an excess of Cr(II)-reducing solution, thus ensuring the reaction progresses to completion. Once all the sulfides are removed, the sulfates were extracted from the residual solution. During extraction sulfur was converted into $H_2S_{(gas)}$ and precipitated as Zn_2S which was in turn converted to Ag_2S using silver nitrate. Approximately 3 mg of Ag_2S were then fluorinated to produce SF_6. The resulting SF_6 was purified through cryogenics and chromatography and analyzed for its multiple sulfur isotope composition on a Thermo Finnigan MAT 253 mass spectrometer.

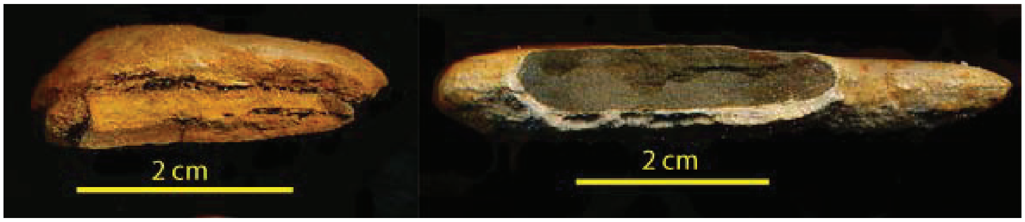

Figure 1.4: Devon Island nodules. The left nodule is more oxidized. The mineralogy of the oxidized nodules consists of pyrite, gypsum, goethite, schwertmannite, and jarosite. The nodule on the right is principally pyrite with a thin coating of gypsum

Results

Sulfide $\delta^{34}S$ values are uniformly negative, and range from -15‰ to -5‰ V-CDT, except for one sample. The associated $\Delta^{33}S$ values are consistently positive, and vary from 0.09‰ to 0.18‰ V-CDT. Sulfate $\delta^{34}S$ values span a greater range (≈ 25‰), from -10‰ to 15‰ V-CDT. The associated $\Delta^{33}S$ values are uniformly positive, and vary from 0.05‰ to 0.19‰ V-CDT. The sulfur isotope measurements for each sulfide-sulfate pair are recorded in table 1.1 and are displayed in a graph in figure 1.5. In a majority of samples, sulfate has different $\delta^{34}S$ and $\Delta^{33}S$ values from the sulfide in the same nodule. Isotopic differences between sulfide and sulfate within individual nodules range from $\varepsilon_{\text{sulfate-sulfide}}$ = -10.1 to +17.9 ‰ (ε is defined as $\delta^{34}S_{\text{sulfate}}$- $\delta^{34}S_{\text{sulfide}}$). For the twelve samples, ε values are summarized in table 1.2.

Sample Name	$\delta^{33}S_{vcdt}$	$\delta^{34}S_{vcdt}$	$\delta^{36}S_{vcdt}$	$\Delta^{33}S_{vcdt}$	$\Delta^{36}S_{vcdt}$
DI-1	-4.31	-8.65	-17.84	0.148	-1.48
DI-1 Sulfate	1.33	2.31	3.32	0.137	-1.08
DI-2	-4.07	-8.18	-17.02	0.149	-1.54
DI-2 Sulfate	1.15	1.98	2.73	0.129	-1.03
DI-3	-3.69	-7.49	-15.82	0.174	-1.63
DI-3 Sulfate	-5.04	-10.14	-21.11	0.193	-1.93
DI-3 Sulfate	-4.80	-9.70	-20.72	0.209	-2.38
DI-4	-5.87	-11.65	-23.55	0.146	-1.53
DI-4 Sulfate	-1.85	-3.77	-8.80	0.098	-1.65
DI-5	-3.97	-8.02	-16.70	0.164	-1.52
DI-5 Sulfate	1.00	1.69	2.23	0.127	-0.99
DI-6	-3.19	-6.41	-13.82	0.116	-1.68
DI-6 Sulfate	2.28	4.32	6.97	0.053	-1.26
DI-7	-3.07	-6.22	-13.38	0.137	-1.60
DI-7 Sulfate	0.62	0.95	0.45	0.126	-1.36
DI-8	7.71	14.87	27.74	0.076	-0.71
DI-8	7.81	15.05	27.99	0.092	-0.79
DI-8 Sulfate	2.51	4.74	7.80	0.069	-1.23
DI-9	-1.62	-3.50	-8.61	0.179	-1.97
DI-9 Sulfate	0.24	0.29	-0.86	0.093	-1.40
DI-10	-7.30	-14.38	-29.00	0.131	-1.85
DI-10 Sulfate	-2.76	-5.62	-12.45	0.141	-1.79
DI-11	-4.08	-8.21	-17.44	0.157	-1.90
DI-11	-3.23	-6.58	-13.27	0.165	-0.81
DI-11 Sulfate	2.13	3.93	6.57	0.114	-0.91
DI-12	-5.65	-11.24	-23.31	0.155	-2.05
DI-12 Sulfate	3.50	6.62	11.92	0.093	-0.70

Table 1.1 : Multiple sulfur isotope data for the 12 nodules. Analytical uncertainty of the measurements is 0.1‰ for $\delta^{34}S$ and 0.01‰ for $\Delta^{33}S$.

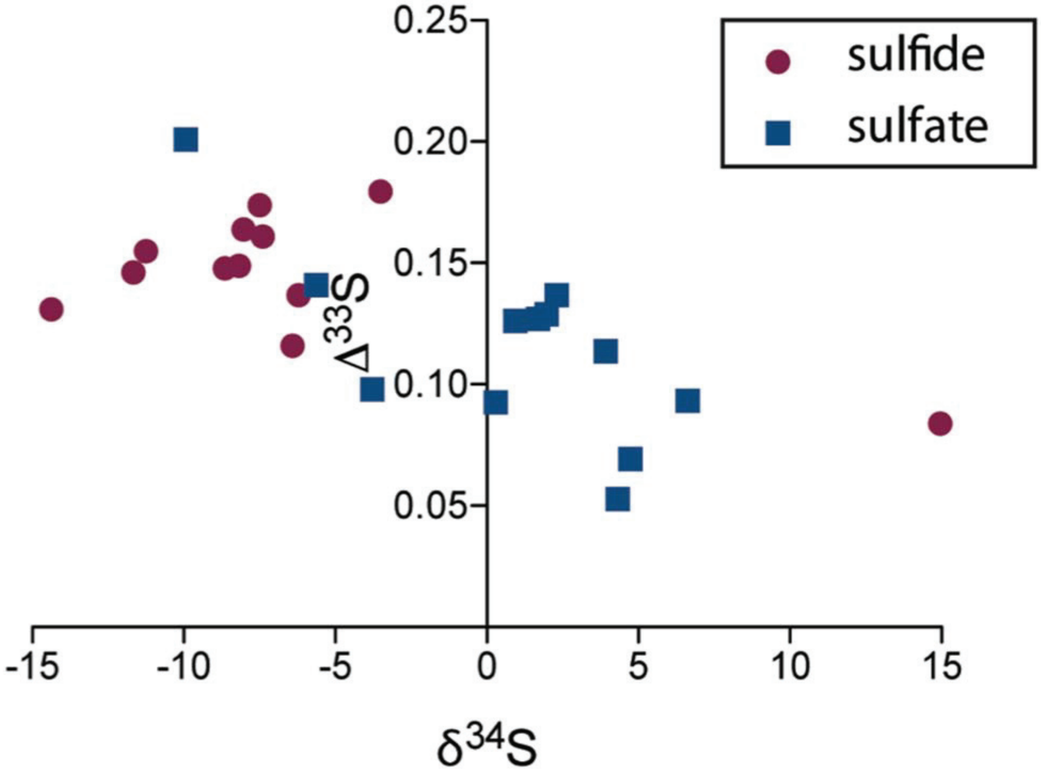

Figure 1.5 : Measured sulfide and sulfate sulfur isotopic composition of Devon Island nodules. Sulfides are in the maroon circles and sulfates are in blue squares. The oxidative products, sulfate, tend to have more positive $\delta^{34}S$.

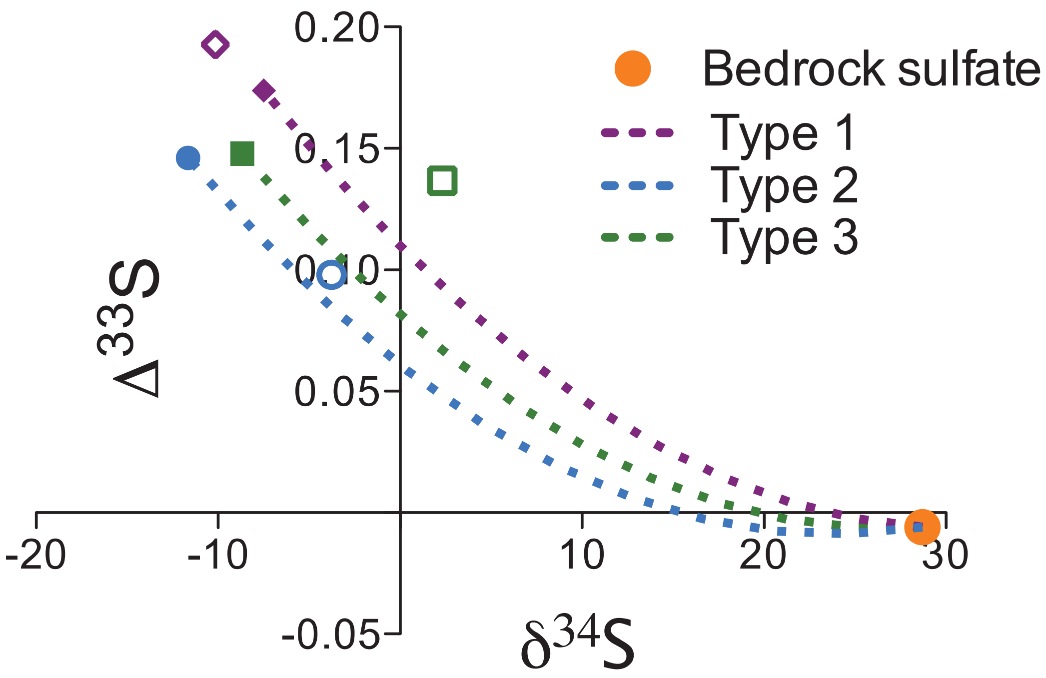

Figure 1.6 : This graph depicts the mixing lines for the two component mixing. Solid symbols represent the sulfide and open symbols corresponding sulfate. Pairs of the same shape and colour are from the same nodule. Three types of sulfide oxidation mechanisms are identified. Type 1: Conventional oxidation (1 sample: DI-3), Type 2: Mixing ~18-30% bedrock sulfate and pyrite (2 samples: DI-4 and DI-6), Type 3: Cannot be explained by conventional oxidation or mixing (9 samples. Above mixing curve: DI-1, 2, 5, 7, 10, 11, and 12. Below mixing curve: DI-8 and DI-9)

Sample Name	**$\varepsilon = \delta^{34}_{sulfate}-\delta^{34}_{sulfide}$**	**Type**
DI-1	10.96	3
DI-2	10.16	3
DI-3	-2.43	1
DI-4	7.89	2
DI-5	9.71	3
DI-6	10.73	2
DI-7	7.17	3
DI-8	-10.22	3*
DI-9	3.79	3*
DI-10	8.76	3
DI-11	11.32	3
DI-12	17.87	3
AVERAGE	7.14	ALL
AVERAGE	10.85	Type 3 samples excluding those marked with *

Table 1.2 : ε values from nodules. ε is defined as product minus reactant. $\delta^{34}_{sulfate}-\delta^{34}_{sulfide}$. The types are defined based on the results of the mixing model. Samples marked with an * are excluded from the type 3 average as they plot below the mixing curve.

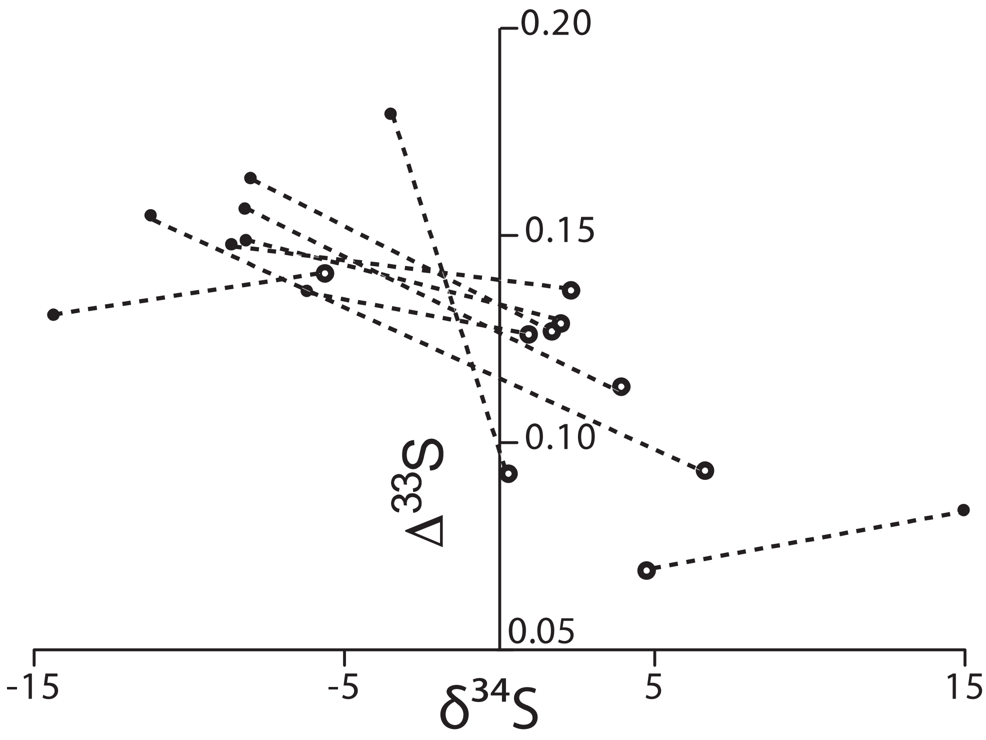

Figure 1.7 : Sulfur isotope values for type 3 samples. Based on the mixing models these samples were identified as type 3. Type 3 samples have the product sulfate above or below the mixing curve. In the above figure solid circles represent sulfide and open circles sulfate. Connecting lines link sulfide-sulfate pairs within the same nodules. Most samples have slightly negative slopes.

Discussion

Many of the observed S-isotope values for pyrite-sulfate pairs presented here are unexpected since little to no sulfur isotope fractionation typically accompanies sulfide oxidation (Brabec et al., 2012; Seal II, 2006). The unusual sulfide-sulfate isotope systematics could indicate a novel fractionation mechanism during low temperature oxidation. However, they may also indicate a more complex process of sulfate mineral formation, where some of the sulfate came from sulfide oxidation and the rest came from a sulfate source with a higher $\delta^{34}S$ value. Finally, equilibrium partitioning of sulfur isotopes should lead to sulfate with higher $\delta^{34}S$ values than co-existing sulfide, superficially similar to the relationships we observe here. These two alternative origins of the observed S-isotope values are explored next.

Mixing of sulfate with high $\delta^{34}S$ values: The lake sediments are found above sulfate-rich bedrock and sulfate-rich breccia from the impact albeit separated by a temporal hiatus (Osinski and Lee, 2005a). Thus, the underlying rocks, and those within the Haughton Impact structure contain mobile sulfate. There sulfur present at Haughton includes pre-impact sulfates, impact breccias, hydrothermal minerals including marcasite and selenite, and weathering products such as gypsum-iron oxide soil crusts (Parnell et al., 2012). There is a wide range of sulfur isotope composition at Haughton ranging from $\delta^{34}S$= -41‰ for marcasite veins to $\delta^{34}S$ +37 ‰ in hydrothermal vent gypsum (Parnell et al., 2012). The previous sulfur work at Haughton does not investigate sulfide-sulfate pairs. The sulfate we measured may reflect a mixture of sulfate produced during sulfide oxidation with this exogenous sulfate source. To evaluate this possibility, we constructed a two-component mixing model between sulfur derived from the sulfide in the nodules and sulfur originating from evaporite beds underlying the Haughton Impact structure. The gypsum bedrock has a sulfur isotopic composition of $\delta^{34}S = 28.7‰$ (Parnell et al., 2010).

The sulfate $\delta^{34}S$ and $\Delta^{33}S$ values from the single type 1 sulfide-sulfate pair appear as expected for conventional sulfide oxidation. A similar process, modified by mixing ~18-30 % sulfate from the gypsum bedrock, can explain the isotopic composition of the two type 2 nodules. Solute transport in cold-region groundwater can occur through a series of freeze, thaw, and evaporation cycles, and would be especially effective if the transporting solutions were sulfate-rich brines (Lacelle and Léveillé, 2010). Therefore, these two samples may be a result of mixing between pyrite and local bedrock sulfate.

The most striking result of our modelling is that the majority of sulfate $\delta^{34}S$ and $\Delta^{33}S$ values cannot be explained by conventional sulfide oxidation or by mixing with the local sulfates.

We have found no simple relationship between sample type and visual indications for oxidation extent. The type 3 oxidative process appears to operate in parallel with conventional sulfide oxidation rather than in some sort of redox sequence. Strong isotopic fractionations are characteristic of type 3 sulfide-sulfate pairs, where the sulfate is enriched in ^{34}S by ~7-18 ‰ relative to the starting sulfide. This type of enrichment is also seen in sulfate-sulfide pairs at isotopic equilibrium. The exponential factor ($^{33}\lambda$) that relates ^{33}S-^{32}S fractionations to ^{34}S-^{32}S fractionations, however, is lower than that expected from isotopic equilibrium in the majority of type 3 samples, with an average $^{33}\lambda$ value of 0.5129 ± 0.0018 (1SD) for the 7 samples that plot above their respective mixing curves.

Equilibrium partitioning of S isotopes: Current temperatures at Devon Island are those of a polar arctic desert and arctic sediment cores indicate that the current "icehouse" cold temperatures have existed since the middle Eocene, (Moran et al., 2006). However, the impact that formed the Haughton Impact Structure produced hydrothermal activity; therefore, for at least several tens of thousands of years after the impact, temperatures in the crater environment were elevated (Osinski et al., 2001). There is no evidence for hydrothermal alteration within the Haughton Formation; therefore, the lake sediments were deposited after cooling post-hydrothermal activity (Osinski and Lee, 2005a). We address the possibility that equilibrium at hydrothermal temperatures could have led to the sulfur isotope systematics that we observe.

Sulfur isotopic equilibrium between SO_4^{2-} and H_2S will be unlikely at temperatures below ~100˚C and at pH >~2 (Ohmoto and Lasaga, 1982).

A two-component S-isotope mixing model was used to evaluate the possibility of mixing between potential sources of sulfur. The two end-members are the pyrite composition of the nodules and the bedrock gypsum. The pyrite composition of the nodules was measured in this study. The sulfur isotopic composition of the bedrock gypsum, measured at $\delta^{34}S = 28.7 \pm 3.6$ ‰, is typical of Ordovician seawater (Parnell et al., 2010). We used a $\Delta^{33}S$ value of -0.006 ± 3.6 ‰ for the model calculations based on values for early Paleozoic seawater sulfate (Wu et al., 2010). Since the sulfate within the Haughton melt rocks was sourced from these evaporites, our choice of this isotopic end member should be representative of this mixing end member as well.

The composition of the mixture is defined by the following equations:

$$
\begin{aligned}
{}^{34}R_{mixture} &= f^{S}_{evaporite}\,{}^{34}R_{evaporite} + f^{S}_{sulfide}\,{}^{34}R_{sulfide} \\
{}^{33}R_{mixture} &= f^{S}_{evaporite}\,{}^{33}R_{evaporite} + f^{S}_{sulfide}\,{}^{33}R_{sulfide} \\
1 &= f^{S}_{evaporite} + f^{S}_{sulfide}
\end{aligned}
$$

In these equations, ${}^{33}R_i$ and ${}^{34}R_i$ represent ${}^{33}S$-${}^{32}S$ and ${}^{34}S$-${}^{32}S$ ratios, normalized to the V-CDT scale, and $f^{S}_{evaporite}$ and $f^{S}_{sulfide}$ represent the relative amount of sulfur in the mixture coming from the evaporite and sulfide end members. We constructed sample-specific mixing curves for each sulfide-sulfate pair by varying $f^{S}_{evaporite}$ between 0 and 1.

The isotopic equilibrium of the nodules is evaluated using equations presented by Otake and colleagues (Otake et al., 2008). Equilibrium, for two minor isotopes ^{33}S and ^{34}S, is calculated between the aqueous species $H_2S_{(aq)}$ and $SO_4^{2-}{}_{(aq)}$ for the following exchange reaction:

$H_2{}^xS + {}^{32}SO_4^{2-} = H_2{}^{32}S + {}^xSO_4^{2-}$ where x= 34 or 33

The equilibrium constant is defined as :

$$K = {}^i\propto_{SO_4^{2-}-H_2S} = {}^i\beta_{SO_4^{2-}} \Big/ {}^i\beta_{H_2S}$$

The theoretical isotopic equilibrium value of the sulfate is calculated using the starting sulfide value (measured pyrite value of the nodule). The value of sulfate in equilibrium with the nodule sulfide is calculated using:

$$\alpha_{i-j}^{34} = {}^{34}_{i}R \Big/ {}^{34}_{j}R = \left(1 + {}^{34}_{i}\delta \Big/ 1000\right) \Big/ \left(1 + {}^{34}_{j}\delta \Big/ 1000\right)$$

α_{i-j} : i=SO_4^{2-} and j=H_2S

Based on calculations, the temperature range at which equilibrium is predicted is inconsistent with the mineralogy present. For example jarosite has a formation temperature ranging from 5-50°C (Madden et al., 2012; Wang et al., 2006). The isotopic equilibrium temperatures calculated from the nodules, despite similar sampling area, are vastly different (ranging from 400 to above 10 000°C).

Additionally, the timing of the deposition of the Haughton Formation is much younger than the impact. Fossil remains in the Haughton Formation favour an early Miocene age ~20 Ma ± 5 Ma (Hickey et al., 1988). This is further supported by field relationships as the Haughton Formation unconformably overlies impact melt breccias in the center of the structure (Osinski and Lee, 2005a). To the south and the west, the Haughton Formation unconformably overlies Lower Paleozoic target rocks (Frisch and Thorsteinsson, 1978; Osinski and Lee, 2005a; Osinski and Lee, 2005b). The basal contact of the Haughton Formation is identified as an unconformity using drill holes (AH98-5 and AH98-6) (Osinski and Lee, 2005a). Reworked impact melt breccias are found as rip-up clasts and minor channel fill (Osinski and Lee, 2005a). The sediment source also supports a hiatus between impact and the Haughton Formation. The impact melt breccias are predominately calcite and silicate glass with or without anhydrite and shocked lithic and mineral clasts (Osinski et al., 2005b) while the Haughton Formation is dominantly dolomite and lacks lithic clasts and shocked minerals (Osinski and Lee, 2005a). Rather than impact breccias, the dolomite-rich member of the Allen Bay Formation is suggested as a sediment source (Osinski and Lee, 2005a). Organic geochemistry also links the hydrocarbon component to the dolomites of the Allen Bay (Parnell et al., 2005). Incorporating the sediment source, the lack of hydrothermal alternation products within the Haughton Formation, age constraints and geological basal contact analysis leads to the conclusion that there was a temporal hiatus of significance separating the impact event and the deposition of the Haughton Formation. There may have been a crater lake formed immediately following the impact; however, evidence of this has since been eroded (Osinski and Lee, 2005a; Osinski and Lee, 2005b; Robertson and Sweeney, 1983).

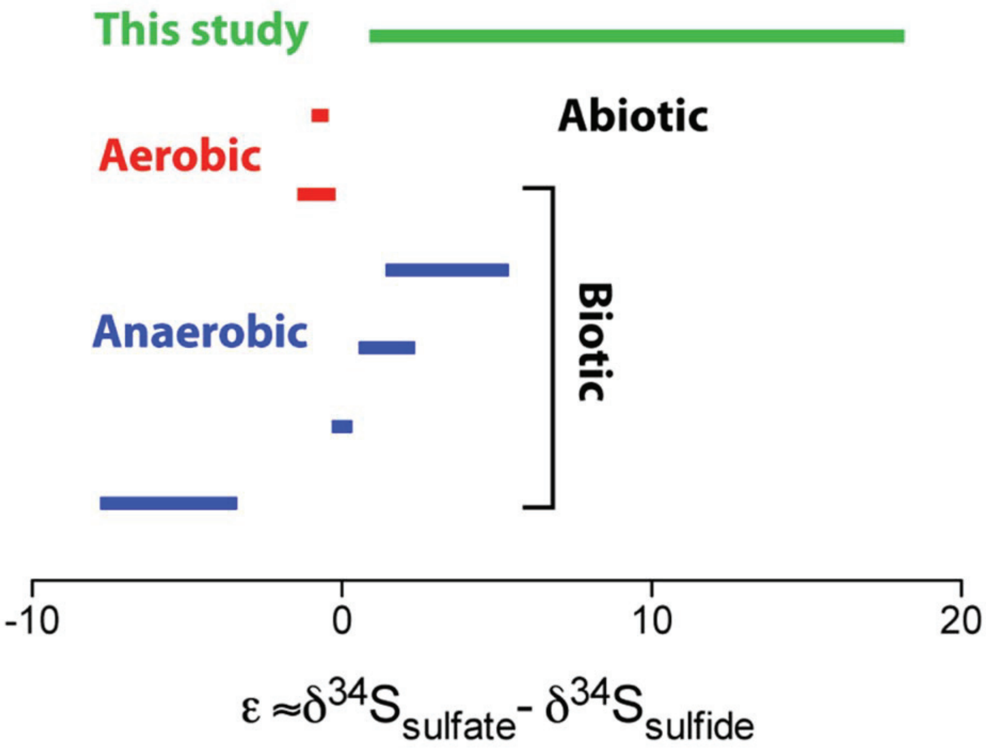

Figure 1.4 : This graph displays several epsilon values reported in the literature for sulfide oxidation. ε is defined as $\delta_{\text{product (sulfate)}}$ minus $\delta_{\text{reactant (sulfide)}}$. The starting reactants are pyrite or aqueous sulfide and the products are sulfate. This study reports epsilon values much larger than previously published suggesting either extreme isotopic amplification by Rayleigh fractionation or the operation of an undiscovered fractionation mechanism. (Balci et al., 2007; Fry et al., 1988; Zerkle et al., 2009)

Biological oxidation and ε values

Our epsilon values are significantly larger than those in the literature (Brabec et al., 2012; Seal II, 2006). Oxidation of sulfur can occur through abiotic processes, biotic processes or a combination of the two. Within our nodules, sulfide, originally as pyrite, is oxidized to a combination of sulfates including gypsum, jarosite, and schwertmannite. Our isotopic data represent an average of either all sulfides or all sulfates within the nodules where multiple mechanisms could be present. In this section, biologically mediated sulfur oxidation reactions are examined. In general, isotopic fractionation during oxidation is quite small even though ^{34}S-sulfide oxidizes more slowly than ^{32}S-sulfide (Fry et al., 1988). For abiotic oxidation the largest fractionation was measured, at 25°C with an average $\varepsilon_{\text{sulfate-sulfide}} = -5.2 \pm 1.4$ ‰ (Fry et al., 1988). A summary of published ε values is found in table 1.3.

Both normal and inverse isotope effects are observed in bacterial sulfide oxidation. Laboratory experiments on anaerobic phototrophs, where sulfide is oxidized to sulfate, show small fractionations. *Allochromatium vinosum,* an anaerobic purple sulfur phototroph, exhibited a $\varepsilon_{\text{sulfate-sulfide}}$of 0.1 ± 0.2 ‰ at 25˚C (Brabec et al., 2012). In contrast, *Chlorobaculum tepidum,* an anaerobic green sulfur phototroph grown at 45˚C, showed an $\varepsilon_{\text{sulfate-sulfide}}$ of -2.3 ± 0.5 ‰ which decreased to -0.7 ± 0.3‰ in later stages of the experiment when sulfate concentrations rose above 0.5 mM (Brabec et al., 2012). In addition, pyrite leaching by *Acidithiobacillus ferrooxidans* causes slight isotopic fractionation $\varepsilon_{\text{sulfate-pyrite}} = -1.3$ ‰ for stoichiometric reactions and $\varepsilon_{\text{sulfate-pyrite}} = +0.4$ ‰ for nonstoichiometric reactions (Pisapia et al., 2007). Breaking the S-S or FeS_2-S bonds could cause this fractionation (Pisapia et al., 2007). Brunner and colleagues measured no isotopic fractionation during pyrite leaching by *A. ferrooxidans*; however, during the initial stage there is a slight enrichment of ^{34}S in the sulfate compared to the initial pyrite (Brunner et al., 2008). According to Brunner et al., degassing of SO_2 depleted ^{34}S could account for this slight enrichment of sulfate early in the reaction stages (Brunner et al., 2008). Anaerobic sulfur oxidation of *A. ferrooxidans* showed small normal fractionations during anaerobic sulfur oxidation both biological (*A. ferrooxidans)* and abiotic ~0.7 ‰ (Balci et al., 2007).

Aerobic oxidation experiments tend to show even smaller fractionations. Aerobic oxidation from FeS_2 to SO_4^{2-} in natural mud samples and laboratory cultures of *Thiobacillus thiooxidans* and *Thiobacillus thioparus* shows no isotopic fractionation (Nakai and Jensen, 1964). Similarly, abiotic and biotic experiments in both submerged and wet/dry experiments show no isotopic fractionation in sulfur but significant fractionation in oxygen (Taylor et al., 1984b). Balci and coworkers measured no isotope fractionation during aerobic oxidation (Balci et al., 2007).

The anoxygenic oxidation of sulfur by the phototroph, *Chlorobium tepidum,* occurs in two steps. The first oxidizing H_2S to S^0 yields a small inverse isotope effect, $\varepsilon_{H2S\text{-}S^\circ}$ = 1 to 2.3 ‰ with an average value of 1.8 ± 0.5 ‰ (Zerkle et al., 2009). The second step is the oxidation of S^0 to SO_4^{2-} which has a small normal isotopic effect with $\varepsilon_{sulfuate\text{-}S^\circ}$ = -1.9 ± 0.8 ‰ with a range of -0.8 to -

3.3 ‰ (Zerkle et al., 2009). $\Delta^{33}S$ for these samples was quite small usually below 0.1‰ (Zerkle et al., 2009).

Published ε values

Abiotic vs Biologic	**Reaction**	**ε**	**Aerobic vs Anaerobic**	**Reference**
Abiotic	Aqueous sulfide	$\varepsilon_{sulfate-sulfide}$= -5.2 ± 1.4‰	Aerobic	(Fry et al., 1988)
Biologic	Photosynthetic bacteria *Chromatium vinosum*	$\varepsilon_{sulfide-S^{\circ}}$ = +2.5 ±0.7‰	Anaerobic	(Fry et al., 1984)
Biologic	*Thiobacillus versutus* oxidation of thiosulfate	Negligible	Aerobic	(Fry et al., 1986)Fry 1986
Biologic	purple sulfur phototrophs *Allochromatium vinosum* (25˚C)	$\varepsilon_{sulfate-sulfide}$= 0.1±0.2‰	Anaerobic	(Brabec et al., 2012)
Biologic	green sulfur phototrophs *Chlorobaculum tepidum* (45˚C)	$\varepsilon_{sulfate-sulfide}$ = -2.3±0.5‰ later decreased to -0.7±0.3‰	Anaerobic	(Brabec et al., 2012)
Biologic	FeS_2 to SO_4^{2-} Natural mud samples	Negligible	Aerobic	(Nakai and Jensen, 1964)
Biologic	FeS_2 to SO_4^{2-} *Thiobacillus thiooxidans* and *Thiobacillus thioparus*	Negligible	Aerobic	(Nakai and Jensen, 1964)
Abiotic	submerged and wet/dry experiments	Negligible	Aerobic and anaerobic	(Taylor et al., 1984a)
Biologic	*Thiobacillus ferroxidans* oxidation of pyrite	Negligible	Aerobic	(Taylor et al., 1984a)
Biologic	*Acidithiobacillus ferrooxidans* Pyrite leaching	$\varepsilon_{sulfate-pyrite}$ = -1.3 to 0.4‰ $\varepsilon_{sulfate-pyrite}$=0‰ $\varepsilon_{sulfate-pyrite}$=-0.7‰	Aerobic	(Pisapia et al., 2007) (Brunner et al., 2008) (Balci et al., 2007)
Abiotic/Biologic	With and without *Acidithiobacillus*	$\varepsilon_{sulfate-pyrite}$=-0.75±0.20	Anaerobic	(Balci et al., 2007)

	ferrooxidans oxidation by $Fe(III)_{aq}$			
Abiotic	oxidation by O_2	$\varepsilon_{sulfate\text{-}pyrite} = -0.1 \pm 0.20$	Aerobic	(Balci et al., 2007)
Biologic	*Acidithiobacillus ferrooxidans*	$\varepsilon_{sulfate\text{-}pyrite} = 0.1 \pm 0.08$	Aerobic	(Balci et al., 2007)
Biologic	*Cholobium tepidum* Step 1 H_2S to S^0	$\varepsilon_{S°\text{-}H2S} = +1.8 \pm 0.5$ ‰,	Anaerobic	(Zerkle et al., 2009)
Biologic	*Cholobium tepidum* Step 2 S^0 to SO_4^{2-}	$\varepsilon_{S°\text{-}sulfate} = -1.9 \pm 0.8$‰	Anaerobic	(Zerkle et al., 2009)

Table 1.3: Published $\varepsilon_{(sulfate\text{-}sulfide)}$ values including both abiotic and biotic as well as anaerobic and aerobic reactions. Sulfur oxidation causes very small fractionation whether anaerobic, aerobic, biological or abiotic.

Whether or not enzymes are involved, kinetic isotope fractionation typically results in normal isotope effects whereas inverse isotope effect can result if an equilibrium process controls the availability of one of the reactants (Fry et al., 1984). An inverse isotope effect was inferred in ten of the twelve nodules. Inverse isotope effects result from isotopic exchange between H_2S and S° or HS^- and H_2S (Fry et al., 1984) while polysulfide intermediates can facilitate the exchange between hydrogen sulfide and elemental sulfide. As isotopic exchange between hydrogen sulfide and the sulfide ion is a function of pH, freeze-thaw cycles may provide a mechanism to amplify the small inverse isotope effects between H_2S and S° or HS^-.

Sulfates produced during phototrophic sulfur oxidation tend to have small negative $\delta^{34}S$ and small positive $\Delta^{33}S$. Larger values are seen with sulfur reduction and sulfur disproportionation with positive $\delta^{34}S$ and negative $\Delta^{33}S$ (Zerkle et al., 2009). Our $\Delta^{33}S$ values, being uniformly positive, are consistent with sulfates produced during phototrophic sulfur oxidation; however, our samples have a greater range of $\delta^{34}S$ values most of which are positive. Therefore, phototrophic sulfur oxidation could not be the sole mechanisms functioning to produce these multiple sulfur isotopic results.

Biosignatures and application to planetary exploration

Large sulfur isotope fractionations associated with sulfide oxidation have implications for planetary exploration of Mars. The Sample Analysis at Mars (SAM) instrument on the Mars Science Laboratory (MSL) Curiosity rover will be able to measure sulfur isotope ratios of Martian samples *in-situ* (Franz et al., 2011). Since microbial sulfate reduction leaves behind a characteristic 'biosignature' in the isotopic composition of its metabolic reactants and products, the ability of SAM to measure sulfur isotopes may help to characterize questions of past Martian habitability.

One issue with this approach is that the strongest isotopic signals are often preserved in sulfide minerals, which may not be long-lived in the oxidizing surface environment of Mars. The previously assumed sulfur isotope consistency implies that potential sulfur isotope biosignatures may be preserved in Martian sulfates despite the intense oxidation on the surface of Mars. While we do not yet have a full understanding of the oxidative mechanism behind our measured unique fractionations, their existence has clear implications for investigating potential biosignatures on the surface of Mars. If low-temperature sulfide oxidation can produce an isotopic enrichment of 10-20 ‰, preservation of potential records of microbial sulfate reduction may be incompatible with the present Martian surface environment, or for that matter, much of its climatic history.

Conclusion

Here we present sulfur isotope fractionation of up to 10-20 ‰ between sulfide and sulfate pairs in sedimentary nodules. Previous experiments with both abiotic and biotic mechanisms show much smaller fractionations generally ranging on the order of -5 to +3.5 ‰ (Brabec et al., 2012; Brunner et al., 2008). Mixing with surrounding sulfate cannot account for the differences in sulfur isotope values observed in most nodules. The nodules are not at equilibrium and geologic evidence indicates a hiatus from underlying sulfur-bearing impact rocks and bedrock. Low temperature sulfide oxidation may have implications on sulfur isotope fractionation. A better understanding of low temperature sulfur oxidation will have implications on the search for biosignatures on Earth, Mars and beyond.

Works Cited

Balci, N., Shanks, W., Mayer, B., Mandernack, K., 2007. Oxygen and sulfur isotope systematics of sulfate produced by bacterial and abiotic oxidation of pyrite. Geochimica Et Cosmochimica Acta 71, 3796-3811.

Brabec, M., Lyons, T., Mandernack, K., 2012. Oxygen and sulfur isotope fractionation during sulfide oxidation by anoxygenic phototrophic bacteria. Geochimica Et Cosmochimica Acta 83, 234-251.

Brunner, B., Yu, J., Mielke, R., MacAskill, J., Madzunkov, S., McGenity, T., Coleman, M., 2008. Different isotope and chemical patterns of pyrite oxidation related to lag and exponential growth phases of Acidithiobacillus ferrooxidans reveal a microbial growth strategy. Earth and Planetary Science Letters 270, 63-72.

Canfield, D.E., 2001. Biogeochemistry of sulfur isotopes, Stable Isotope Geochemistry, pp. 607-636.

Chambers, L., Trudinger, P., 1978. Microbiological fractionation of stable sulfur isotopes - review and critique. Geomicrobiology Journal 1, 249-293.

Fossing, H., Jorgensen, B., 1989. Measurement of bacterial sulfate reduction in sediments - evaluation of a single-step chromium reduction method Biogeochemistry 8, 205-222.

Franz, H.B., Mahaffy, W., Kasprzak, E., Lyness, E., Raaen, E., 2011. Measuring sulfur isotope ratios from solid samples with the Sample Analysis at Mars instrument and the effects of dead time corrections, 42nd Lunar and Planetary Science Conference, the Woodlands, Texas, pp. 2800-2801.

Frisch, T., Thorsteinsson, R., 1978. Haughton astrobleme: Mid-Cenozoic impact crater Devon Island, Canadian Arctic archipelago. Arctic 31, 108-124.

Fry, B., Cox, J., Gest, H., Hayes, J.M., 1986. Discrimination between 34S and 32S during bacterial metabolism of inorganic sulfur compounds. Journal of Bacteriology 165, 328-330.

Fry, B., Gest, H., Hayes, J.M., 1984. Isotope effects associated with the anaerobic oxidation of sulfide by the purple photosynthetic bacterium, Chromotium vinosum. Fems Microbiology Letters 22, 283-287.

Fry, B., Ruf, W., Gest, H., Hayes, J., 1988. Sulfur isotope effects associated with oxidation of sulfide by O2 in aqueous solution. Chemical Geology 73, 205-210.

Hickey, L.J., Johnson, K.R., Dawson, M.R., 1988. The Stratigraphy, Sedimentology, and Fossils of the Haughton Formation: A Post-Impact Crater-Fill Devon Island, N.W.T., Canada. Meteoritics 23, 221-231.

Kaplan, I.R., Rittenberg, S.C., 1964. Microbiological fractionation of sulphur isotopes. Journal of General Microbiology 34, 195-212.

Lacelle, D., Léveillé, R., 2010. Acid drainage generation and associated Ca–Fe–SO4 minerals in a periglacial environment, Eagle Plains, NorthernYukon, Canada: A potential analogue for low-temperature sulfate formation on Mars Planetary and space science 58, 509-522.

Léveillé, R., 2007. Formation of Jarosite and Mars-Like Minerals in a Polar Desert: Implications for Mars Aqueous Geochemistry. GSA Denver Annual Meeting.

Madden, M., Madden, A., Rimstidt, J., Zahrai, S., Kendall, M., Miller, M., 2012. Jarosite dissolution rates and nanoscale mineralogy. Geochimica Et Cosmochimica Acta 91, 306-321.

Mayr, R.T.U., 1987. The Sedimentary Rocks of Devon Island, Canadian Arctic Archipelago in: Geological Survey of Canada (Ed.). Minister of Supply and Services. Ottawa, Ontario, Canada.

Moran, K., Backman, J., Brinkhuis, H., Clemens, S., Cronin, T., Dickens, G., Eynaud, F., Gattacceca, J., Jakobsson, M., Jordan, R., Kaminski, M., King, J., Koc, N., Krylov, A., Martinez, N., Matthiessen, J., McInroy, D., Moore, T., Onodera, J., O'Regan, M., Palike, H., Rea, B., Rio, D., Sakamoto, T., Smith, D., Stein, R., St John, K., Suto, I., Suzuki, N., Takahashi, K., Watanabe, M., Yamamoto, M., Farrell, J., Frank, M., Kubik, P., Jokat, W., Kristoffersen, Y., 2006. The Cenozoic palaeoenvironment of the Arctic Ocean. Nature 441, 601-605.

Nakai, N., Jensen, M., 1964. The kinetic isotope effect in the bacterial reduction and oxidation of sulfur. Geochimica Et Cosmochimica Acta 28, 1893-1912.

Ohmoto, H., Lasaga, A., 1982. Kinetics of reactions between aqueous sulfates and sulfides in hydrothermal systems. Geochimica Et Cosmochimica Acta 46, 1727-1745.

Osinski, G., Lee, P., 2005a. Intra-crater sedimentary deposits at the Haughton impact structure, Devon Island, Canadian High Arctic. Meteoritics & Planetary Science 40, 1887-1899.

Osinski, G., Lee, P., Spray, J., Parnell, J., Lim, D., Bunch, T., Cockell, C., Glass, B., 2005a. Geological overview and cratering model for the Haughton impact structure, Devon Island, Canadian High Arctic. Meteoritics & Planetary Science 40, 1759-1776.

Osinski, G., Spray, J., 2003. Evidence for the shock melting of sulfates from the Haughton impact structure, Arctic Canada. Earth and Planetary Science Letters 215, 357-370.

Osinski, G., Spray, J., Lee, P., 2001. Impact-induced hydrothermal activity within the Haughton impact structure, arctic Canada: Generation of a transient, warm, wet oasis. Meteoritics & Planetary Science 36, 731-745.

Osinski, G., Spray, J., Lee, P., 2005b. Impactites of the Haughton impact structure, Devon Island, Canadian High Arctic. Meteoritics & Planetary Science 40, 1789-1812.

Osinski, G.R., Lee, P., 2005b. Intra-crater sedimentary deposits at the Haughton impact structure, Devon Island, Canadian High Arctic Meteoritics & Planetary Science 40, 1887-1899.

Osinski, G.R., Lee, P., Spray, J.G., Parnell, J., Lim, D.S.S., Bunch, T.E., Cockell, C.S., Glass, B., 2005c. Geological overview and cratering model for the Haughton impact structure, Devon Island, Canadian High Arctic. Meteoritics & Planetary Science 40, 1759-1776.

Otake, T., Lasaga, A., Ohmoto, H., 2008. Ab initio calculations for equilibrium fractionations in multiple sulfur isotope systems. Chemical Geology 249, 357-376.

Parnell, J., Boyce, A., Osinski, G., Izawa, M., Banerjee, N., Flemming, R., Lee, P., 2012. Evidence for life in the isotopic analysis of surface sulphates in the Haughton impact structure, and potential application on Mars. International Journal of Astrobiology 11, 93-101.

Parnell, J., Boyce, A., Thackrey, S., Muirhead, D., Lindgren, P., Mason, C., Taylor, C., Still, J., Bowden, S., Osinski, G., Lee, P., 2010. Sulfur isotope signatures for rapid colonization of an impact crater by thermophilic microbes. Geology 38, 271-274.

Parnell, J., Lee, P., Osinski, G., Cockell, C., 2005. Application of organic geochemistry to detect signatures of organic matter in the Haughton impact structure. Meteoritics & Planetary Science 40, 1879-1885.

Pisapia, C., Chaussidon, M., Mustin, C., Humbert, B., 2007. O and S isotopic composition of dissolved and attached oxidation products of pyrite by Acidithiobacillus ferrooxidans: Comparison with abiotic oxidations. Geochimica Et Cosmochimica Acta 71, 2474-2490.

Robertson, P., Sweeney, J., 1983. Haughton Impact Structure: structural and morphological aspects. Canadian Journal of Earth Sciences 20, 1134-1151.

Seal II, R.R., 2006. Sulfur Isotope Geochemistry of Sulfide Minerals. Reviews in Mineralogy and Geochemistry, pp. 633-677.

Sherlock, S., Kelley, S., Parnell, J., Green, P., Lee, P., Osinsk, G., Cockell, C., 2005. Re-evaluating the age of the Haughton impact event. Meteoritics & Planetary Science 40, 1777-1787.

Sim, M., Bosak, T., Ono, S., 2011. Large Sulfur Isotope Fractionation Does Not Require Disproportionation. Science 333, 74-77.

Taylor, B., Wheeler, M., Nordstrom, D., 1984a. Isotope composition of sulfate in acid-mine drainage as measure of bacterial oxidation. Nature 308, 538-541.

Taylor, B., Wheeler, M., Nordstrom, D., 1984b. Stable isotope geochemistry of acid-mine drainage -experimental oxidation of pyrite. Geochimica Et Cosmochimica Acta 48, 2669-2678.

Thode, H., 1991. Sulfur Isotopes in Nature and the Environment: An Overview, in: Krouse, H., Grinkenko, V. (Eds.), Stable Isotopes: Natural and Anthropogenic Sulphur in the Environment. John Wiley & Sons, Chicester, New York, Brisbane, Toronto, Singapore, pp. 1-26.

Toran, L., Harris, R., 1989. Interpretation of sulfur and oxygen isotopes in biological and abiological sulfide oxidation. Geochimica Et Cosmochimica Acta 53, 2341-2348.

Wang, H., Bigham, J., Tuovinen, O., 2006. Formation of schwertmannite and its transformation to jarosite in the presence of acidophilic iron-oxidizing microorganisms. Materials Science & Engineering C-Biomimetic and Supramolecular Systems 26, 588-592.

Wu, N., Farquhar, J., Strauss, H., Kim, S.-T., Canfield, D.E., 2010. Evaluating the S-isotope fractionation associated with Phanerozoic pyrite burial Geochimica et Cosmochimica Acta 74, 2053-2071.

Zerkle, A., Farquhar, J., Johnston, D., Cox, R., Canfield, D., 2009. Fractionation of multiple sulfur isotopes during phototrophic oxidation of sulfide and elemental sulfur by a green sulfur bacterium. Geochimica Et Cosmochimica Acta 73, 291-306.

Connection

The previous chapter focused on mass dependent processes. Measurements of multiple sulfur isotopes in both sulfide and sulfates within oxidizing nodules are used to elucidate information regarding the formation processes. Samples are from another Canadian environment –Devon Island in Nunavut. Very large fractionations up to almost 20 ‰ are measured between sulfide and sulfate. These results cannot be explained by conventional oxidation or mixing with bedrock sulfate. Low-temperature oxidation may have some novel mechanisms causing these large fractionations. There are implications for the preservations of "biosignatures" on Earth and other planets if oxidation can cause large fractionations.

The following chapter moves back in time into the section of $\Delta^{33}S$ versus time where mass independent fractionation prevails. The aim of this chapter is to investigate the Mesoarchaean minimum for lithological and geographical biases. I was able to expand on the previous published Mesoarchaean range in both $\Delta^{33}S$ and $\delta^{34}S$ measurements. In addition, previously the systematics of the Mesoarchaean seemed to be different from other Archaean data leading to the development of complex atmospheric models to explain the change. The Mesoarchaean samples were more horizontally distributed when graphed in $\Delta^{33}S$ versus $\delta^{34}S$ compared to Eo, Paleo, and Neoarchaean samples which have diagonal displacement as well as horizontal (Archaean reference array). This dataset adds another geographic location, Canada, to the previously investigated Mesoarchaean terranes of Australia and South Africa. In addition, the samples show a diminished version of the Archaean reference array, with samples distributed along a positive diagonal in $\Delta^{33}S$ versus $\delta^{34}S$ space, which has been interpreted as the products of atmospheric reactions. Deviations in horizontal distribution are attributed to microbial processing.

Lithologic and geographic test of the Mesoarchaean S-MIF minimum

K.J. Rodzinyak and B.A. Wing

Introduction

Mass independent fractionation of sulfur isotopes (S-MIF) is an anomalous enrichment or depletion in ^{33}S-^{32}S and ^{36}S-^{32}S isotope ratios relative to what would be expected from associated ^{34}S-^{32}S ratios. Experiments demonstrate that photodissociation of SO_2 gas results in S-MIF (Farquhar et al., 2000a; Farquhar et al., 2001). Under ultraviolet radiation, the SO_2 molecule dissociates by the following reaction: $SO_2 + h\nu \rightarrow SO + O$ (Farquhar et al., 2001), with photodissociation of the sulfur monoxide ultimately producing elemental sulfur. Relative to the starting sulfur dioxide, the product elemental sulfur is anomalously enriched in ^{33}S, and depleted in ^{36}S, leaving the residual SO_2 anomalously depleted in ^{33}S and enriched in ^{36}S (Farquhar et al., 2000a).

The geological and biological processes of Earth's surface sulfur cycle enabled atmospheric sulfur aerosols, sulfate aerosols, and sulfur dioxide to influence the isotopic composition of sulfide and sulfate minerals prior to ≈2400-2500 Ma (Farquhar et al., 2000a; Ono et al., 2003). . For example, atmospheric sulfate aerosols are soluble and appear to have transferred S-MIF to the oceanic sulfate reservoir in the Archaean Eon (Farquhar and Wing, 2003). In turn, microbial sulfate reduction seems to have sequestered this oceanic S-MIF signature in pyrite (Ono et al., 2003). The fate of the S-MIF carried by elemental sulfur is more complex, with elemental sulfur reducing bacteria, reaction with iron oxyhydroxide, or isotopic exchange with aqueous sulfide potentially carrying the S-MIF into sedimentary sulfides (Farquhar and Wing, 2003; Ono et al., 2003).

The disappearance of S-MIF around ≈2400 to 2500 Ma (Farquhar et al., 2000a) is broadly contemporaneous with other proxies that have long been taken to indicate increasing levels of atmospheric oxygen, including the appearance of red beds, disappearance of banded iron formation, and lack of detrital uraninite and pyrite grains (Cloud, 1972, 1973). This synchroneity is not coincidental, as atmospheric oxygen likely played a key control on the production and preservation of S-MIF on the Archaean Earth.

The production constraint occurs when enough oxygen accumulates in the atmosphere to produce a significant ozone shield and ozone blocks out the ultraviolet rays necessary for the photodissociation of sulfur dioxide (Farquhar et al., 2000b). In addition, even if photodissociation of sulfur dioxide can occur, the resulting elemental sulfur will undergo oxidative photochemistry, potentially preventing S-MIF preservation. At atmospheric oxygen abundances > 10^{-5} Present Atmospheric Levels (PAL; ≈21%), elemental sulfur species will be reoxidized to sulfate, erasing any S-MIF in the sulfate ocean reservoir (Pavlov and Kasting, 2002). In essence, for MIF preservation, sulfur needs to be removed from the atmosphere in a variety of oxidation states; for this to occur a reducing atmospheric environment must be present (Kasting et al., 1989).

The temporal distribution of the S-MIF record exhibits a distinct binary structure, as illustrated by the variation of $\Delta^{33}S$[1] measurements with time (Fig. 1). This structure is conventionally taken to reflect a rise in atmospheric oxygen at ≈2400 to 2500 Ma that passed a threshold and shut off processes producing and preserving S-MIF. However, apart from the broad binary structure representing the switch from a low-oxygen to an oxygenated

---

[1] $\Delta^{33}S$ values express the deviation of measured ^{33}S-^{32}S ratios from those expected on the basis of measured ^{34}S-^{32}S ratios and are calculated as: $\Delta^{33}\mathrm{S} = \delta^{33}\mathrm{S} - 1000 \times \left(\left(\frac{\delta^{34}\mathrm{S}}{1000} + 1 \right)^{0.515} - 1 \right)$

atmosphere, there are finer scale variations within the Archaean S-MIF record. The clearest of these shows up in the variable range of $\Delta^{33}S$ values through the Archaean (Figure 2.1).

Within the Eoarchaean (3600 to 3850 Ma) and Paleoarchaean (3200 to 3600 Ma) eras, $\Delta^{33}S$ values cover a range of 7.5 ‰. At the other of the eon, the largest magnitudes in both positive and negative $\Delta^{33}S$ values occur in the Neoarchaean era (2500 to 2800 Ma) ranging over 13.4 ‰. However, there is a significant decrease in the magnitudes of $\Delta^{33}S$ values within the Mesoarchaean era (2800 to 3200 Ma), with a range of only 1.8 ‰ (Farquhar et al., 2007; Ohmoto et al., 2006). The presence of this bowtie structure in the $\Delta^{33}S$ record has led to much speculation about the processes that control S-MIF variability in the middle Archaean.

The diminished $\Delta^{33}S$ variability has been attributed primarily to atmospheric compositional changes. Mesoarchaean fluctuations in atmospheric oxygen have been proposed; such a "yo-yo" earth hypothesis invokes atmospheric oxygen present in high enough levels to cause reoxidation of sulfur species within the atmosphere leading to a dilution effect on S-MIF (Ohmoto et al., 2006). A Mesoarchaean high-altitude methane haze might work to diminish $\Delta^{33}S$ variability. When atmospheric CO_2/CH_4 ratios are greater than 0.1 in sophisticated photochemical models, a high-altitude methane haze forms and block out the ultraviolet radiation driving to sulfur dioxide photodissociation (Domagal-Goldman et al., 2008). Variations in the ratio of outgassed volcanic SO_2 to H_2S could be a contributing factor as well. The ratio of atmospheric SO_2 to H_2S affects S-MIF because H_2S photodissociation does not lead to significant S-MIF in the ultimate photochemical products (Farquhar et al., 2000a). In basic terms, adding more H_2S to the atmosphere while keeping SO_2 levels constant will dilute the S-MIF signal produced by SO_2 photodissociation (Halevy et al., 2010). However, the published Mesoarchaean multiple sulfur isotope dataset exhibits two features that suggest caution may be warranted about speculation on the atmospheric consequences of the Mesoarchaean $\Delta^{33}S$ minimum.

First, $\Delta^{33}S$ measurements have only been made on middle Archaean samples from essentially two geographic regions: the Transvaal basin from the Kaapvaal Craton in South Africa and the Hamersley basin from the Pilbara Craton in Australia (Figure 2.2). Paleomagnetic reconstructions combined with stratigraphic similarities (Cheney, 1996) place the Kaapvaal and Pilbara cratons in close proximity in the Vaalbara supercontinental reconstruction (de Kock et al., 2012; de Kock et al., 2009). One implication of these reconstructions is that the Hamersley basin and the Transvaal basin may represent a single depositional basin as far back as 3.6 Ga (Zegers et al., 1998). If these reconstructions hold true, then for global isotope studies, rock samples from outside the Pilbara and Kaapvaal cratons should be examined. Although the Mesoarchaean paleogeography of the Superior craton is not well constrained, available geological data place it in a separate cratonic ‘clan’ from the Pilbara and Kaapvaal cratons (BLEEKER, 2002). In summary, the shared geochemical and geological evolution of the Pilbara and Kaapvaal cratons (Kaufman et al., 2007) raises the question of whether the Mesoarchaean $\Delta^{33}S$ minimum reflects peculiar local conditions rather than a global process.

In addition, the lithologic distribution of much of the published Mesoarchaean dataset is poorly known (Figure 2.3). Of the samples for which lithologic information is available, most are shales interpreted to be of lacustrine or marine origin (Figure 2.3; (Ohmoto et al., 2006). The lithologic monotony of the current Mesoarchaean $\Delta^{33}S$ record suggests that the possibility of a lithologic control on the Mesoarchaean $\Delta^{33}S$ minimum remains to be evaluated. In order to constrain the geographic and lithologic distribution of the diminished Mesoarchaean S-MIF signal, we obtained multiple S isotope data from a variety of lithologies from previously uninvestigated Mesoarchaean terrains of the Superior Province in Northern Ontario, Canada. We aimed to test if the Mesoarchaean $\Delta^{33}S$ minimum is a primary signal of sulfur cycling in the contemporaneous surface environment or whether it results from a geographic and lithologic sampling bias. In order to evaluate these hypotheses, we constructed a multiple sulfur isotope database from 33 papers of published Archaean sulfur isotope measurements.

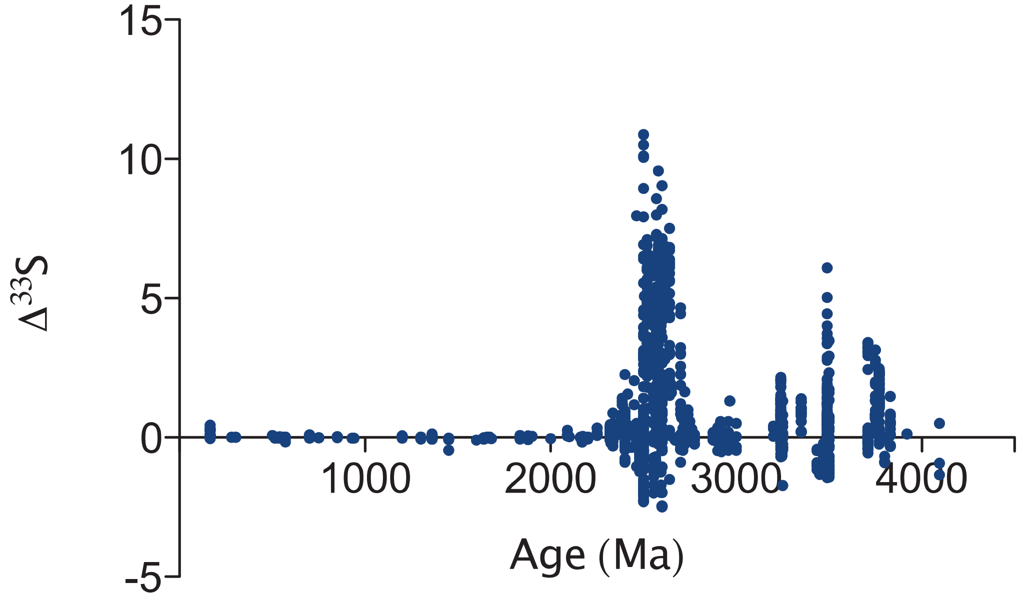

Figure 2.1 : Compilation of published $\Delta^{33}S$ values versus time. Samples interpreted to reflect sulfides of ambiguous or detrital origin were excluded from the plot. Around ≈2400-2500 Ma there is a shift to near zero $\Delta^{33}S$ values. The cluster of smaller magnitude $\Delta^{33}S$ values around 3000 Ma reflects the Mesoarchaean minimum that we focus on here.

(Bao et al., 2007; Baublys et al., 2004; Bekker et al., 2004; Cates and Mojzsis, 2006; Domagal-Goldman et al., 2008; Farquhar et al., 2000a; Farquhar et al., 2007; Golding et al., 2011; Guo et al., 2009; Hou et al., 2007; Hu et al., 2003; Jamieson et al., 2006; Johnston et al., 2008; Johnston et al., 2006; Johnston et al., 2005; Mojzsis et al., 2003; Ohmoto et al., 2006; Ono et al., 2006a; Ono et al., 2003; Ono et al., 2009a; Ono et al., 2009b; Papineau and Mojzsis, 2006; Papineau et al., 2007; Partridge et al., 2008; Philippot et al., 2007; Rouxel et al., 2008; Shen et al., 2009; Thomazo et al., 2009; Ueno et al., 2008; Whitehouse et al., 2005; Williford et al., 2011; Zerkle et al., 2012)

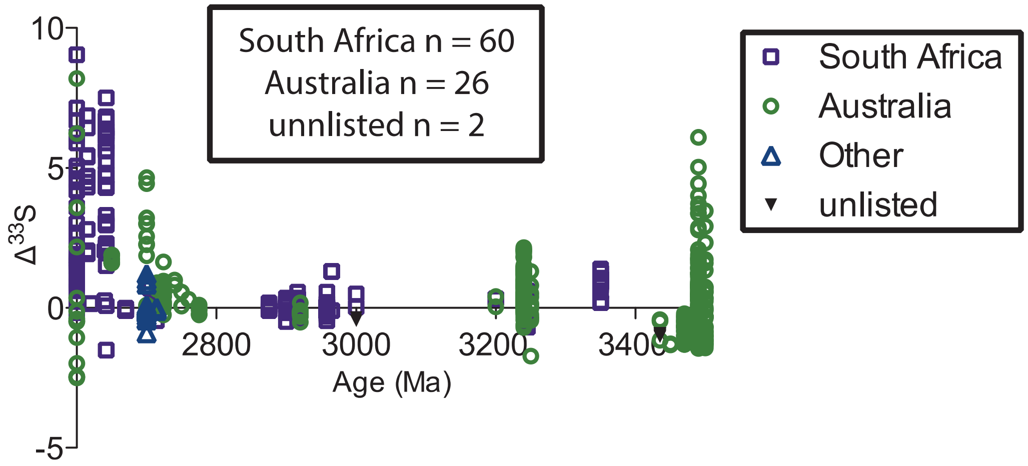

Figure 2.1: Geographic distribution of published middle Archaean $\Delta^{33}S$ values. Throughout this time period, analyzed samples have dominantly come from Archaean rocks in South Africa and Australia. Numbers of samples listed include only those from the Mesoarchaean era (2800-3200 Ma).

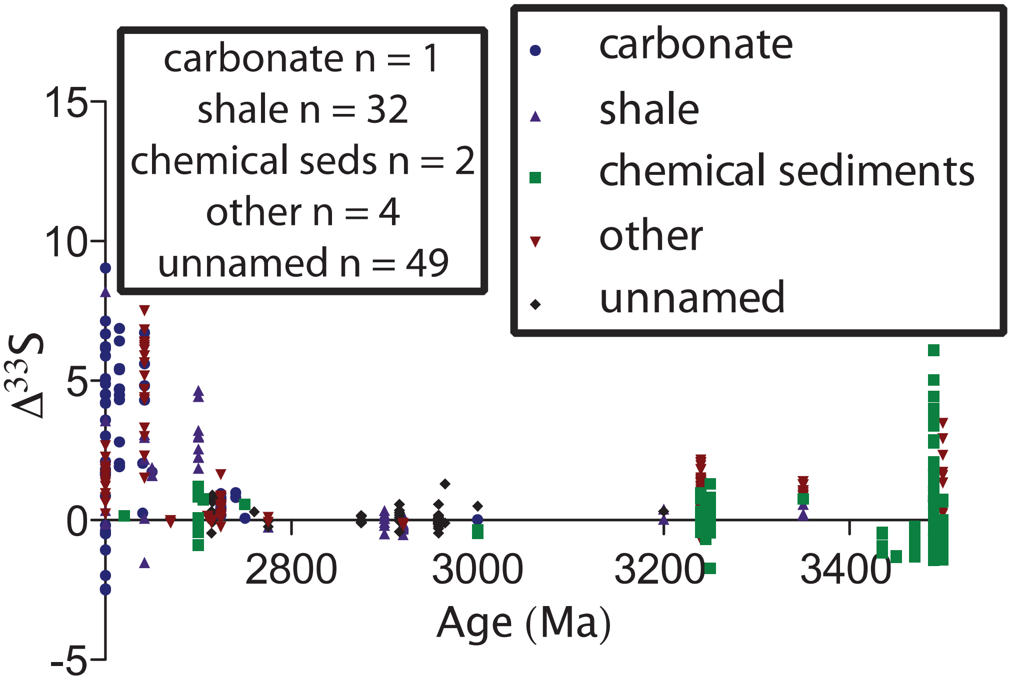

Figure 2.2: Lithologic distribution of published middle Archaean $\Delta^{33}S$ values. Throughout the Mesoarchaean era, analyzed samples are dominantly of unknown lithologic affinity or come from shales in Australia. Numbers of samples listed include only those from the Mesoarchaean era (2800-3200 Ma).

Geological Background

We sampled greenstone belts in Northwestern Ontario that exposed Archaean rocks within the timeframe of the Mesoarchaean $\Delta^{33}S$ minimum. The sampled rock packages are all between 2800-3000 Ma old, and include a variety of lithologies, including metavolcanic and metasedimentary rocks. This allowed us to collect rocks of similar ages that were formed in different depositional environments. All the greenstone belts – Finlayson Lake, Lumby Lake, Red Lake and Woman Lake – are within the Superior Province, one of the Archaean provinces in the northern part of Laurentia. The Superior Province along with other Archaean provinces were sutured together in the early Proterozoic eon (Hoffman, 1988). Sampled rocks were metamorphosed to upper greenschist facies in places (Buse et al., 2009).

Lumby Lake

The Lumby Lake greenstone belt is within the dominantly metaplutonic Marmion terrane within the Western Wabigoon subprovince (Fig. 4; (Tomlinson et al., 1998). Structurally at the south margin there is a belt-scale thrust fault which was subsequently sheared dextrally (Buse et al., 2010). The Lumby Lake volcano-sedimentary assemblage is between 3014 and 2830 Ma (Buse et al., 2009, 2010). This greenstone belt is interpreted to result from subduction plume-modified oceanic spreading centers and possible mantle plume activity on the subduction zone (Buse et al., 2009). Plume-driven mafic and komatiitic volcanism in the Lumby Lake area occurred around 2828±2 Ma (Tomlinson et al., 2003). The depositional sequences in the greenstone belt are from south to north: Lumby South, Bar Lake, Pinecone, and Lumby North (Buse et al., 2010).

The south younging sequence has ages ranging from 2963 to 3016 Ma (Tomlinson et al., 2003). Within the Lumby Lake greenstone belt, zircons from tonalite gneiss from the Marmion batholith have ages from 2.898-3.003 Ma (Tomlinson et al., 2003). Uranium-lead analyses of zircons from two felsic tuffs and a quartz porphyry yield a mean age of 2999 ± 1 Ma (Davis and Jackson, 1988) while U-Pb ages ranging from 2828±2 to 3014 ±1 Ma are seen from zircon in felsic tuffs (Tomlinson et al., 2003). Age measurements (U-Pb) from a felsic tuff within komatiite flows and iron formation of the Pinecone assemblage give an age of 2828.3 ± 1.8 Ma (Tomlinson et al., 2003).

Lumby Lake sediments indicate a shallowing deposition environment (Fralick et al., 2008), with the clastic sediments representing a distal equivalent to the turbidite sequence identified in the Finlayson Lake area (King, 1998). The fault-offset upper Lumby Lake sedimentary sequence has been linked to the upper Finlayson Lake sequence based on similarities in chemical composition of sedimentary rocks, which indicates source rocks of the same composition (Fenwick, 1976; King, 1998; Stone and Pufhal, 1995).

Samples collected are from the Pinecone assemblage. These include principally shales and sulfide-rich shales as well as some banded iron formations, tuffs and pillow basalts. An age of 2828 is measured from a felsic tuff within this assemblage (Tomlinson et al., 2003).

Red Lake

The Red Lake greenstone belt is on the south margin of the ≈3000 Ma North Caribou terrane (Fig. 4), and contains volcano-sedimentary assemblages ranging in age from 2992 to 2733 Ma (Corfu and Andrews, 1987; Corfu et al., 1998; Corfu and Stott, 1993; Corfu and Wallace, 1986). The oldest age comes from felsic volcanics in the eastern part of the belt that overlie the tholeiitic to komatiitic sequence while the youngest ages come from calc-alkaline volcanics in the northern part of the belt (Corfu and Wallace, 1986) . Assemblages within the Red Lake greenstone belt of Mesoarchaean age reflect primarily plume magmatism (2990-2960 Ma) followed by arc magmatism (2940-2910 Ma) and sedimentation from 2890-2900 Ma (Sanborn-Barrie et al., 2001). Overall, the supracrustal rocks are interpreted to represent deposition in a sediment-starved marine basinal setting (Sanborn-Barrie et al., 2001).

We sampled rocks from the Balmer, Slate Bay, Ball and Bruce Channel assemblages. The Balmer assemblage ranges from 2990-2960 Ma based on U-Pb ages on zircons from felsic flows (Corfu and Andrews, 1987; Corfu and Wallace, 1986). The Balmer assemblage is dominated by tholeiitic and komatiitic lava flows with iron formations (Tomlinson et al., 1998). The Slate Bay consisting of wacke-mudstones with polymictic conglomerates is ≤2916 ± 4 Ma (Corfu et al., 1998). Supracrustal rocks in the Slate Bay assemblage are dominantly clastics, with wacke-mudstones intercalated with polymictic conglomerates (Corfu et al., 1998). Mafic volcanics and felsic pyroclastic rocks dominate the Ball assemblage with local cherty horizons and stromatolite-bearing dolomite marbles (Hofmann et al., 1985). U-Pb ages on volcanics bracket one stromatolitic bed between 2940 and 2923 Ma (Corfu et al., 1998). Consisting principally of basalt with minor felsic tuffs, the Bruce Channel assemblage ≈ 2894 also contains clastic sedimentary rocks and iron formations Ma (Corfu et al., 1998).

Finlayson Lake

The Finlayson Lake greenstone belt trends northeast-southwest and lies northwest of the Marmion shear zone (Fig. 4) (Stone, 2008). The rocks of Finlayson Lake are mainly foliated mafic flows and banded amphibolites with thin units of felsic tuffs and metasediments

(Tomlinson et al., 2003). These metasediments consist of iron formation, shales and cherts followed by sandstones and conglomerates (King, 1998). A U-Pb zircon age from a quartz-feldspar porphyritic tuff is 2931.4 ±2.0 Ma. Lower in the stratigraphy, outcropping on the southern part of Finlayson lake, U-Pb ages give an age range of 2997± 2.5 Ma to 3003 ± 0.7 Ma from detrital zircon in a conglomerate and a quartz-feldspar porphyry volcanic respectively (Stone, 2008).

Samples collected in 2010 are associated from the northern shore or the central Snake Island and the date of 2931.4 from a felsic tuff is used for these samples. Samples analyzed from those collected in 2011 are from the southern part of the lake and the older date of 2997-3003 Ma is used (Stone, 2008). An average of this range is used when graphing samples. Lithologies sampled include phyllite, greywacke, carbonate, chert, sandstone, pillow basalt, and pyrite nodule.

Woman Lake

The Woman Lake greenstone belt is situated within the east-central part of the Uchi subprovince (Figure 2.4) (Corfu et al., 1998). The Uchi-Confederation Lakes Greenstone belts are divided into three cycles of volcanism with the oldest represented by a crystal tuff dated at 2958.6 ± 1.7 Ma and the youngest by a rhyolite dated at 2738 +5/-2 Ma (Nunes and Thurston, 1980). The Woman lake greenstone belt is cut by dikes aged 2832 Ma, giving a minimum age of deposition (Rogers, 2002) . Woman Lake assemblages consist of ignimbrites, tuffaceous rhyolites and dacitic flows, pillowed mafic flows, stromatolitic limestones, iron formations and siltstones (Rogers, 2002). The stromatolites have been interpreted to have formed in shallow water conditions within the photic zone (Hofmann et al., 1985). The updated age calculated by Rogers from a felsic tuff horizon at 2871 Ma is used for the age of the Woman Lake samples (Rogers, 2002). Lithologies of samples collected include rhyolite, chert, carbonates, banded iron formation, and pillow basalts.

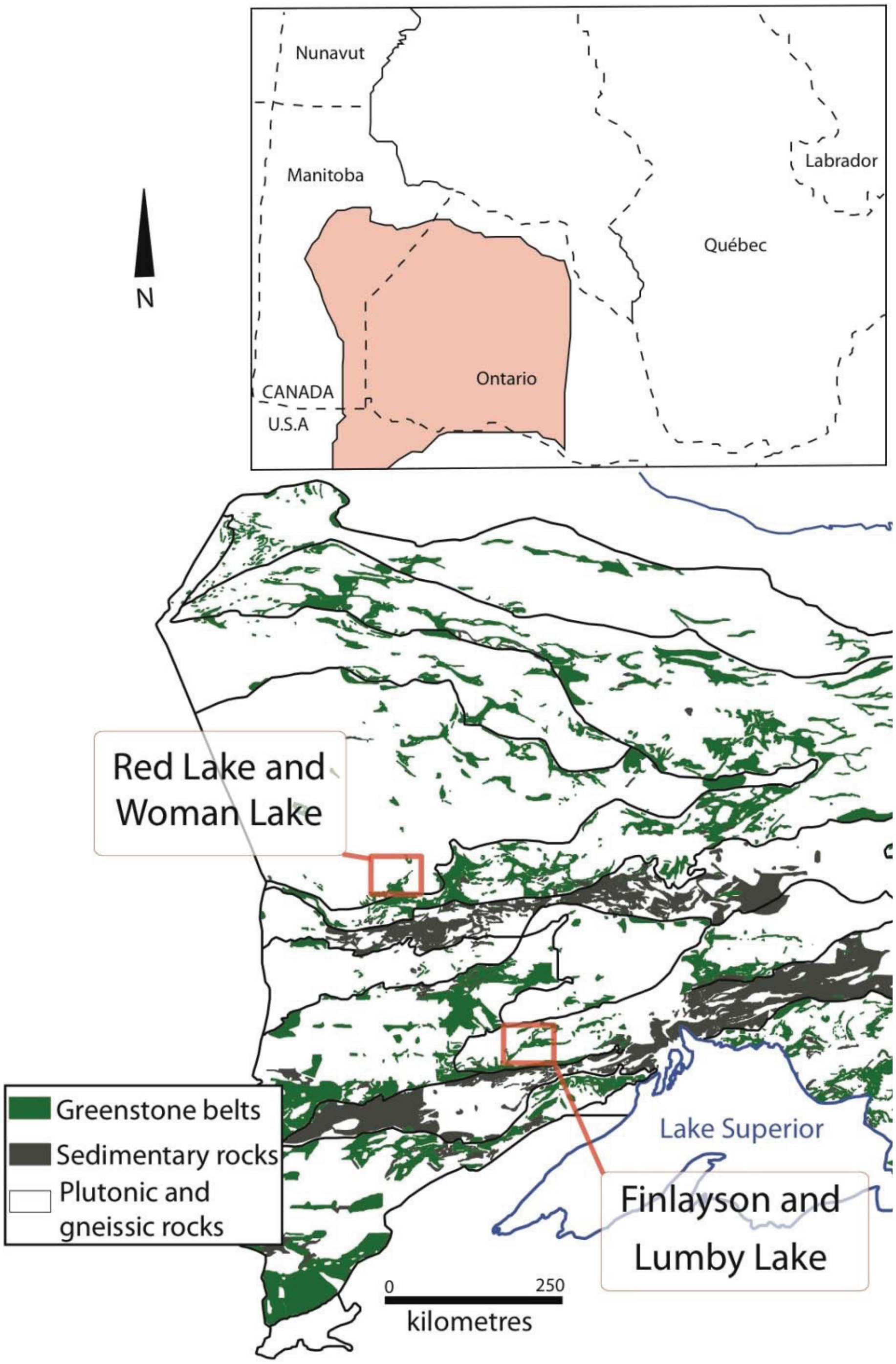

Figure 2.4 : Locations of sampled greenstone belts. Terrane boundaries shown as thick black lines and are unlabeled for clarity. Simplified from Figure 20.1 in (Stott et al., 2010).

Methods

Whole rock samples were crushed and ground to powder after sawing off weathered surfaces and fractured regions. Where sulfides were visible to the naked eye, they were sometimes hand drilled with a Dremel. Sulfides were selectively extracted through an acid-volatile sulfur / chrome-reducible sulfur (AVS/CRS) extraction procedure modified after (Canfield et al., 1986). Carbonate samples with low sulfide contents were first digested with 12 N HCl and the residual powder was dried prior to the AVS/CRS extractions. During the extractions, sulfide sulfur was separated from the rocks as H_2S, which was carried by N_2 gas though a trap filled with 4% zinc acetate solution trapping the H_2S as ZnS. Approximately 0.2 mL 0.1N $AgNO_3$ solution was then added to the zinc acetate trap, converting the ZnS to Ag_2S. The Ag_2S was washed with 5 mL 1N NH_4OH, filtered, and dried overnight at approximately 70 °C.

We analyzed the sulfur isotope composition of the Ag_2S following established procedures (Ono et al., 2006b). In brief, approximately 3 mg of Ag_2S were fluorinated to produce SF_6. The resulting SF_6 was purified cryogenically and chromatographically. Purified SF_6 was analyzed for its multiple sulfur isotope composition by monitoring the SF_5^+ ion beam at m/z = 127 ($^{32}SF_5^+$), 128 ($^{33}SF_5^+$), 129 ($^{34}SF_5^+$), and 131 ($^{36}SF_5^+$) on a Thermo MAT 253 mass spectrometer. Sulfur isotope compositions are expressed as δ values on the V-CDT scale (Ding et al., 2001):

$$\delta^{x}S = \left[\frac{\left(S^{x}/S^{32}\right)_{\mathrm{sample}}}{\left(S^{x}/S^{32}\right)_{\mathrm{V-CDT}}} - 1\right]$$

where *x* refers to 33, 34, or 36 and the measured value is multiplied by a factor of 1000 to look at variations in per mil quantities. The $\delta^{34}S$ value of the international standard IAEA-S-1 is defined to be -0.3 ‰ on the V-CDT scale. We also use Δ values to examine the presence of S-MIF in our samples. For Δ^{33}S values we have:

$$\Delta^{33}\mathrm{S} = \delta^{33}\mathrm{S} - 1000 \times \left(\left(\frac{\delta^{34}\mathrm{S}}{1000} + 1\right)^{0.515} - 1\right)$$

and for Δ^{36}S values we have:

$$\Delta^{36}\mathrm{S} = \delta^{36}\mathrm{S} - 1000 \times \left(\left(\frac{\delta^{34}\mathrm{S}}{1000} + 1\right)^{1.90} - 1\right)$$

We look at Δ^{33}S and Δ^{36}S variations in per mil quantities also. We take the Δ^{33}S value of IAEA-S-1 to be 0.094 ‰ and the Δ^{36}S value to be -0.70 ‰.

The sulfur isotope database compiles published literature data. Since a variety of definitions for Δ^{33}S are in publications all measurements are converted to the same definitions used in the sulfur isotope terminology section. Sample lithology when not listed directly in the paper was taken by matching the depths to published drill core logs (Schroder et al., 2006). For comparison samples which were identified as detrital or ambiguous in origin were excluded.

Results

Sulfide δ^{34}S values range from -4.6‰ to 8.9‰ V-CDT, while the associated Δ^{33}S values range from -0.93‰ to 2.32‰ V-CDT. Samples with significant Δ^{33}S values also have Δ^{36}S values that fall on a slope of approximately -1, which is typical for Archaean S-MIF. The clastic rocks in our sample suite exhibit near-zero Δ^{33}S values, while the chemically/biologically precipitated rocks preserve significant S-MIF.

Macroscopic pyrites within some samples show resolvable differences in their multiple S isotope compositions. For example, the silica-rich layers, in a BIF from Lumby Lake, have more positive $\delta^{34}S$ and $\Delta^{33}S$ values compared to the silica-poor layers. Silica-rich layer has a $\delta^{34}S$ of 1.12‰ and a $\Delta^{33}S$ of 1.01‰ compared to the silica-poor with $\delta^{34}S$ of -0.17‰ and $\Delta^{33}S$ of 0.59‰.

Macroscopic pyrites are extracted separately from surrounding matrix. For example, in a black carbonate from Red Lake $\Delta^{33}S$ are comparable with 0.23‰ in pyrite and 0.20‰ in carbonate. $\delta^{34}S$ are 0.38‰ and 0.99‰, respectively. Similarly in a siliceous argillite $\Delta^{33}S$ are 0.05‰ and 0.06‰ in concentrated pyrite and massive. But the $\delta^{34}S$ shows greater variability with 0.14‰ and -0.55‰. Other samples contain different types of sulfides with similar isotopic compositions. Chalcopyrite and pyrite grains within a single VMS sample, for example, show negligible difference in their multiple S isotope compositions. Concentrated sulfide deposits have the largest range of multiple sulfur isotopes.

Field Samples Data Table

Sample	Age	$\delta^{33}S$	$\delta^{34}S$	$\delta^{36}S$	$\Delta^{33}S$	$\Delta^{36}S$	Lithology	GPS	
FL 2010 1A	2997-3003	0.02	0.11	0.38	-0.040	0.16	fine-grained, quartz rich greywacke	602337	5416539
FL 2010 1A	2997-3003	-0.53	-0.93	-1.55	-0.047	0.22	fine-grained, quartz rich greywacke	602337	5416539
FL 2010 1A	2997-3003	-0.47	-0.82	-1.76	-0.043	-0.20	fine-grained, quartz rich greywacke	602337	5416539
FL 2010 1A background	2997-3003	-0.01	0.04	0.42	-0.028	0.35	fine-grained, quartz rich greywacke	602337	5416539
FL 2010 1D pyrite	2997-3003	-0.43	-0.38	-0.02	-0.233	0.71	pyrite in black carbonate	602337	5416539
FL 2010 1D background	2997-3003	-0.71	-0.99	-1.46	-0.198	0.41	background of black carbonate	602337	5416539
FL 2010 1E	2997-3003	-1.90	-2.49	-4.41	-0.623	0.31	pyrite nodule	602337	5416539
FL 2010 2B	2997-3003	0.66	0.50	0.32	0.406	-0.80	graded bed	602337	5416539
FL 2010 2B	2997-3003	0.62	0.46	0.08	0.378	-0.80	graded bed	602337	5416539
FL 2010 2C	2997-3003	-0.48	-0.85	-1.45	-0.048	0.16	chlorite rich with quartz fine grained phyllite	602337	5416539
FL 2010 2D	2997-3003	1.43	2.42	4.35	0.178	-0.26	phyllite	602337	5416539
FL 2010 3A	2997-3003	0.49	0.57	0.74	0.203	-0.34	phyllite	602337	5416539
FL 2010 3A	2997-3003	0.48	0.48	0.65	0.235	-0.26	phyllite	602337	5416539
FL 2010 4D	2997-3003	1.70	2.61	4.68	0.357	-0.28	pyrite in wacke	603264	5417481
FL 2010 6A	2997-3003	0.45	0.65	0.98	0.113	-0.25	volcanic tuff	603375	5417652
FL 2011 1E (2)	2997	-3.29	-4.57	-7.61	-0.930	1.06	concentrated sulfide	602985	5416541
FL 2011 1E	2997	-2.76	-3.91	-6.38	-0.739	1.04	concentrated sulfide	602985	5416541
LL 2010 1A	2825-2829	1.06	0.58	0.43	0.763	-0.67	black shale	633065	5435601
LL 2010 1A	2825-2829	1.02	0.53	0.40	0.746	-0.61	black shale	633065	5435601
LL 2010 1A	2825-2829	0.85	0.19	0.08	0.748	-0.29	black shale	633065	5435601
LL 2010 2A	2825-2829	1.55	3.22	6.20	-0.105	0.08	BIF	632319	5435707
LL 2010 2C	2825-2829	2.53	2.88	4.53	1.049	-0.95	BIF	632319	5435707
LL 2010 3B	2825-2829	3.55	8.08	16.14	-0.610	0.72	pillow basalt margin	632987	5436786

LL 2010 3C	2825-2829	3.87	8.94	17.73	-0.719	0.68	Pillow basalt within pillow	632987	5436786
LL 2010 3D	2825-2829	3.14	7.36	14.80	-0.648	0.76	within pillow with lighter crystals	632987	5436786
LL 2011 2B	2825-2829	1.61	2.77	5.28	0.185	0.02	pyritized shale	632300	5436834
LL 2011 2C	2825-2829	1.65	0.94	1.06	1.161	-0.73	pyritized shale	632300	5436834
LL 2011 2D	2825-2829	2.72	3.12	5.28	1.110	-0.66	pyritized shale	632300	5436834
LL 2011 3A	2825-2829	2.23	1.95	2.61	1.227	-1.09	BIF	632223	5436930
LL 2011 5E light layers	2825-2829	1.59	1.12	1.06	1.012	-1.07	BIF	633481	5438807
LL 2011 5E dark layers	2825-2829	0.50	-0.17	-0.63	0.588	-0.31	BIF	633481	5438807
RL 2010 1A	2996	-0.35	-0.81	-1.60	0.063	-0.06	greywacke	444730	5665958
RL 2010 1A	2996	-0.15	-0.45	-0.85	0.082	-0.01	greywacke	444730	5665958
RL 2010 1A	2996	-0.47	-1.05	-2.19	0.076	-0.19	greywacke	444730	5665958
RL 2010 1A	2996	-0.53	-1.19	-2.53	0.083	-0.27	greywacke	444730	5665958
RL 2010 1A	2996	-0.27	-0.66	-1.57	0.067	-0.32	greywacke	444730	5665958
RL 2010 1C (massive)	2996	0.12	0.14	0.50	0.050	0.23	silicified argillite	444730	5665958
RL 2010 1C (veins)	2996	-0.22	-0.55	-0.76	0.064	0.29	pyrite veins in argillite	444730	5665958
RL 2010 1D	2996	-0.64	-1.20	-2.30	-0.024	-0.01	massive sulfide	444730	5665958
RL 2010 1D	2996	2.73	5.44	10.63	-0.064	0.28	massive sulfide	444730	5665958
RL 2010 1D (iridescent)	2996	-0.68	-1.34	-2.97	0.011	-0.42	massive sulfide	444730	5665958
RL 2010 1D (pyrite)	2996	-0.66	-1.15	-2.81	-0.071	-0.63	massive sulfide	444730	5665958
RL 2010 1D	2996	-0.53	-1.02	-2.20	0.001	-0.26	massive sulfide	444730	5665958
RL 2010 2A	2996	1.34	2.63	4.96	-0.020	-0.05	very fine dark carbonate with sulfides	412091	5654629
RL 2010 2C	2996	0.63	2.21	4.81	-0.508	0.62	chert	412091	5654629
RL 2010 2D	2996	3.74	8.49	17.59	-0.620	1.40	massive sulfide	412091	5654629
RL 2010 4A background	2996	3.02	1.46	0.02	2.267	-2.76	graphitic shale	415282	5650687
RL 2010 4A pyrite	2996	3.58	2.46	2.32	2.316	-2.36	graphitic shale	415282	5650687

RL 2011 1B	2996	0.97	1.71	2.26	0.087	-0.99	chert	419780	5654598
RL 2011 2B	2996	1.42	4.93	11.24	-1.118	1.86	carbonate	419734	5654625
RL 2011 2C	2996	-0.88	0.23	2.13	-1.001	1.70	carbonate	419734	5654625
RL 2011 10A	2996	1.64	4.06	7.63	-0.449	-0.10	carbonate	421885	5655813
WL 2011 11A	2871	0.62	1.34	2.39	-0.067	-0.16	pillow basalt	514150	5661755

Figure 2.3 : Data for the Mesoarchaean samples from this study. Samples acronyms correspond with sampling locations. FL: Finlayson Lake, LL: Lumby Lake, RL: Red Lake, WL: Woman Lake. GPS coordinates are in UTM NAD 83. Analytical uncertainty of the measurements is 0.1‰ for $\delta^{34}S$ and 0.01‰ for $\Delta^{33}S$.

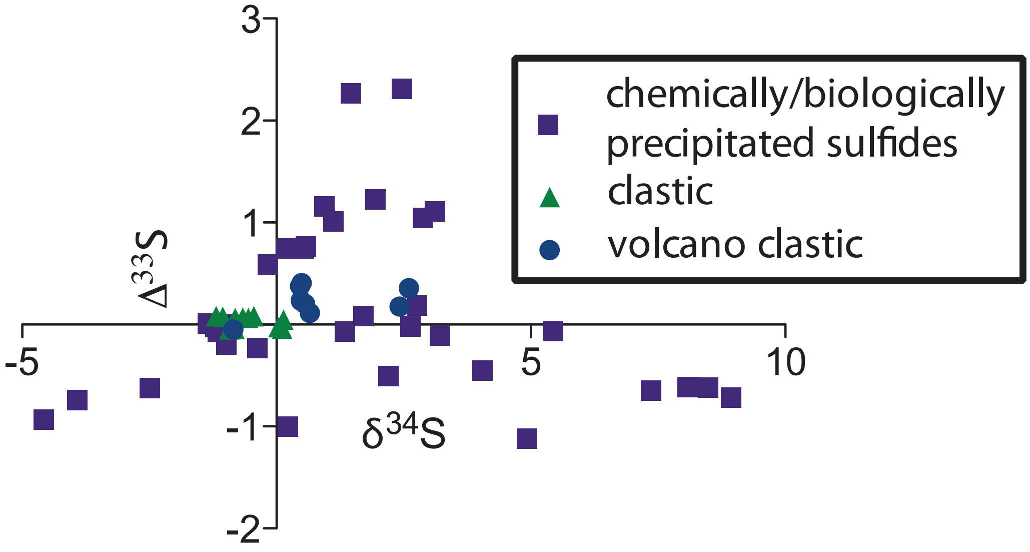

Figure 2.6 : Data compiled in this study. There is a distinct control of lithology on the magnitude of $\Delta^{33}S$. Samples which have been biologically or chemically precipitated show the large variations in both $\Delta^{33}S$ and $\delta^{34}S$.

Sulfides in pillow basalt, both chilled rims and the interior of pillows, have $\delta^{34}S$ ranging from 7.36 to 8.94‰ and $\Delta^{33}S$ from -0.61 to -0.72‰. The largest $\Delta^{33}S$ corresponds to the largest $\delta^{34}S$. In general, shales tend to have both positive $\Delta^{33}S$ and positive $\delta^{34}S$. In addition, banded iron formations tend to have positive $\Delta^{33}S$ and positive $\delta^{34}S$. Conversely, carbonates have negative $\Delta^{33}S$ and a range of $\delta^{34}S$.

In comparison to published literature data, this dataset measures greater range in both $\Delta^{33}S$ and $\delta^{34}S$. Furthermore, the shape of the distribution is more similar to the previously published Archaean array which has been used to describe the sulfur isotope systematics for Eo, Paleo and Neoarchaean. This Archaean array is diagonal displacement interpreted as sourcing from the atmosphere as well as horizontal variability from microbial processing.

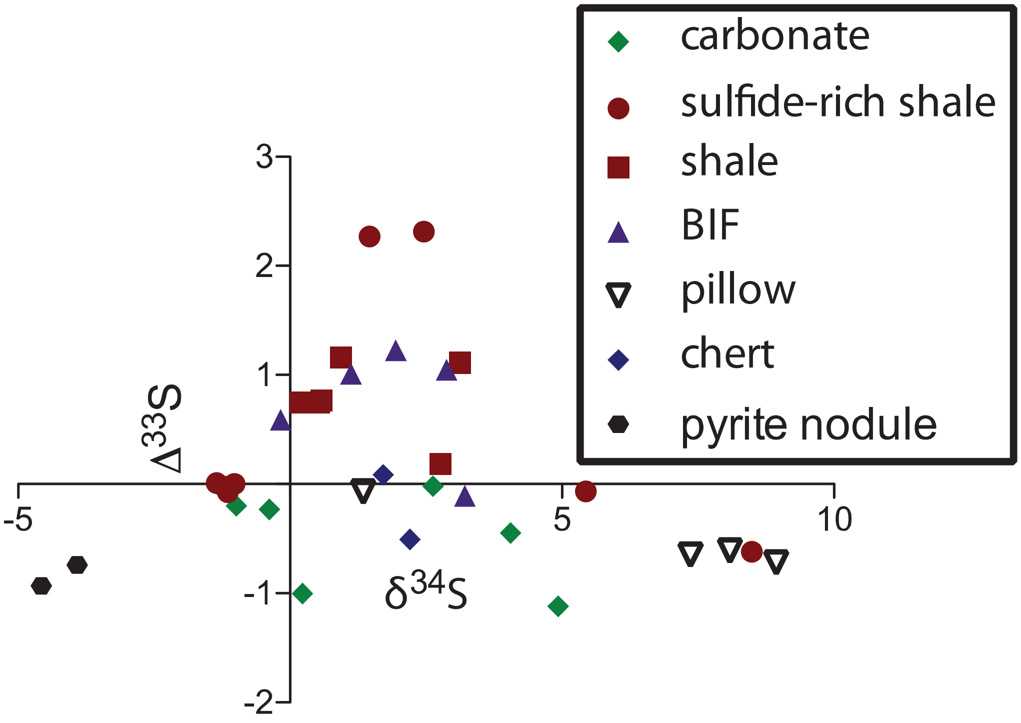

Figure 2.7 : Detailed lithology of chemically and biologically precipitated sulfides.

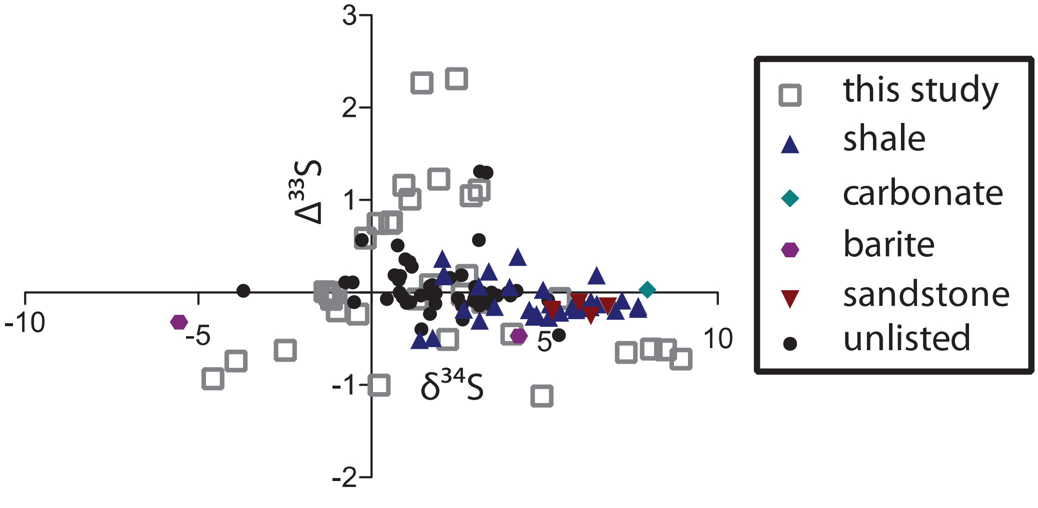

Figure 2.8 : Published literature data overlain on this dataset. The range of this study extends the range of measured multiple sulfur isotopes for the Mesoarchaean. (Domagal-Goldman et al., 2008; Farquhar et al., 2000a; Farquhar et al., 2007; Ohmoto et al., 2006; Ono et al., 2006b)

There are two analytical methods used to obtain the multiple sulfur isotope data: the ion microprobe or the mass spectrometer. With the ion microprobe single spots on a single crystal can be analyzed. With the chemical extraction method coupled with the mass spectrometer an average of the sulfides within the sample are taken. In order to compare similar analyses types only bulk extraction analyses are used. The literature Mesoarchaean data plots more horizontally in $\Delta^{33}S$ versus $\delta^{34}S$ compared to the data presented in this study which has more of the diagonal trend observed in other Archaean eons.

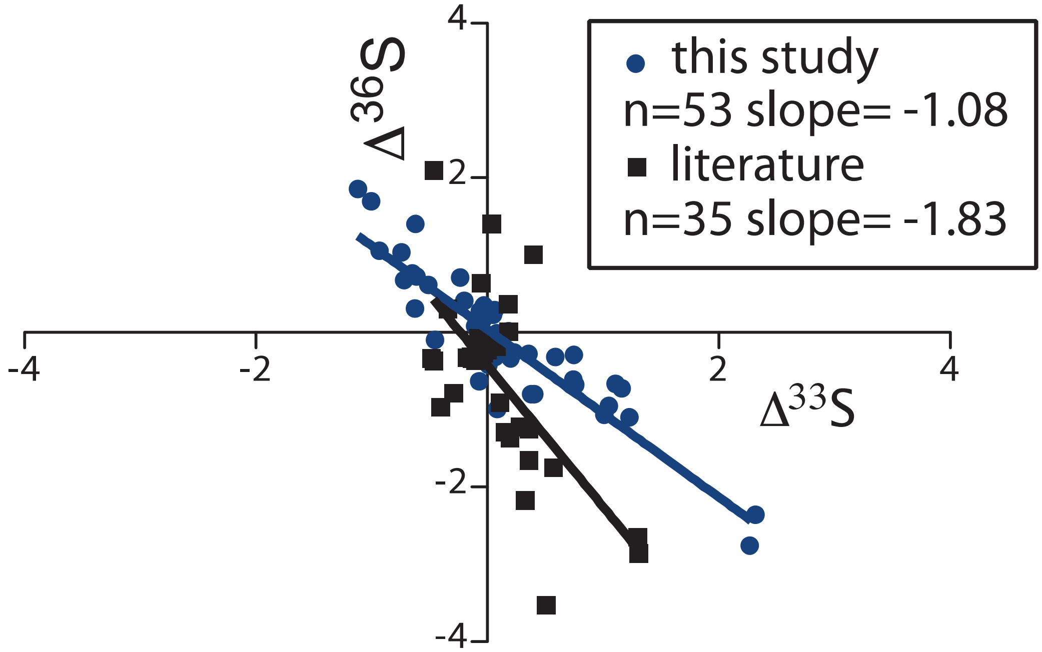

Figure 2.9 : $\Delta^{33}S$ versus $\Delta^{36}S$. Literature data from (Farquhar et al., 2000a; Farquhar et al., 2007; Ono et al., 2006a)

Discussion

Compared to literature data for the Mesoarchaean, we observe a slightly larger spread in both $\delta^{34}S$ and $\Delta^{33}S$ values. The overall S-MIF range is still reduced relative to the rest of the Archaean. The identification of diminished S-MIF range in multiple localities and lithologies (including shales, carbonates, cherts, and BIFs) suggests that this is a primary feature of the Mesoarchaean atmosphere rather than the effect of sampling bias. This interpretation is supported by the lithologic controls on S-MIF preservation that we have identified here.

Despite the reduced S-MIF magnitude, the updated Mesoarchaean sulfur isotope distribution shows similar systematics to other parts of the Archaean. The observed $\Delta^{33}S$ and $\delta^{34}S$ variability can be explained by covariation along the Archaean reference array (Figure 2.10) and a horizontal spread of $\delta^{34}S$ values all with similar -$\Delta^{33}S$ values (Ono et al., 2003). The Archaean reference array forms an acute angle when comparing $\Delta^{33}S$ and $\delta^{34}S$ variability. Diagonal variability is interpreted to result from sampling products from atmospheric photolysis reactions which generate mass independent fractionation. Variations horizontally (changes in $\delta^{34}S$ of samples with negative $\Delta^{33}S$) are from mass dependent processes such as microbial processing. Samples from the previous Mesoarchaean data form a horizontal cluster offset from the origin slightly towards the positive $\delta^{34}S$ values (Figure 2.11a). However, when including the dataset from this study a diminished acute angle emerges (Figure 2.11b). The interpretations attributed to the Archaean reference array should now be applicable to the Mesoarchaean, albeit taking into consideration the contracted magnitude.

Another distinguishing feature of multiple sulfur isotopes in the Archaean is the characteristic slope of -1. The Archaean covariation of $\Delta^{33}S$ and $\Delta^{36}S$ occurs in mass independent processes such as sample gas-phase reactions. Hitherto, Mesoarchaean samples were identified as distinct from other Archaean periods (Farquhar et al., 2007); however, the samples in this study have a slope of -1. These features suggest that the diminished Mesoarchaean S-MIF record may be best explained through dilution by a S source without S-MIF, either in the atmosphere or in the marine reservoir, rather than by changing the photochemical regime producing S-MIF.

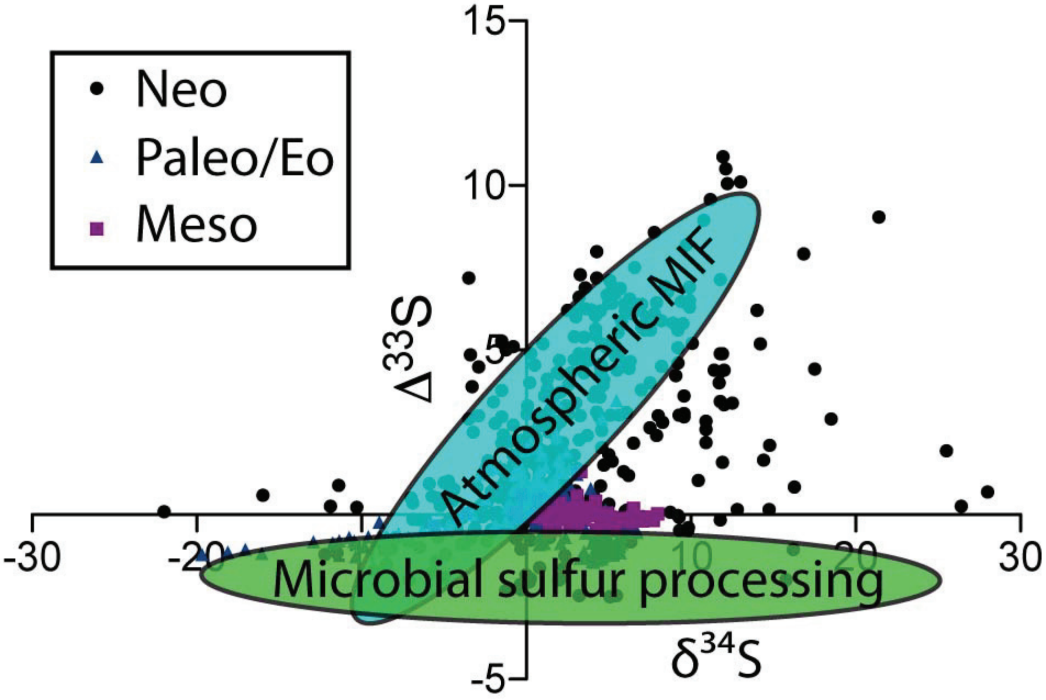

Figure 2.10 : Archaean reference array. Deviations along the diagonal are interpreted as samples which contain products from atmospheric reactions producing mass independent fractionation. Distribution horizontally along the x-axis is mass dependent and attributed to microbial processes.

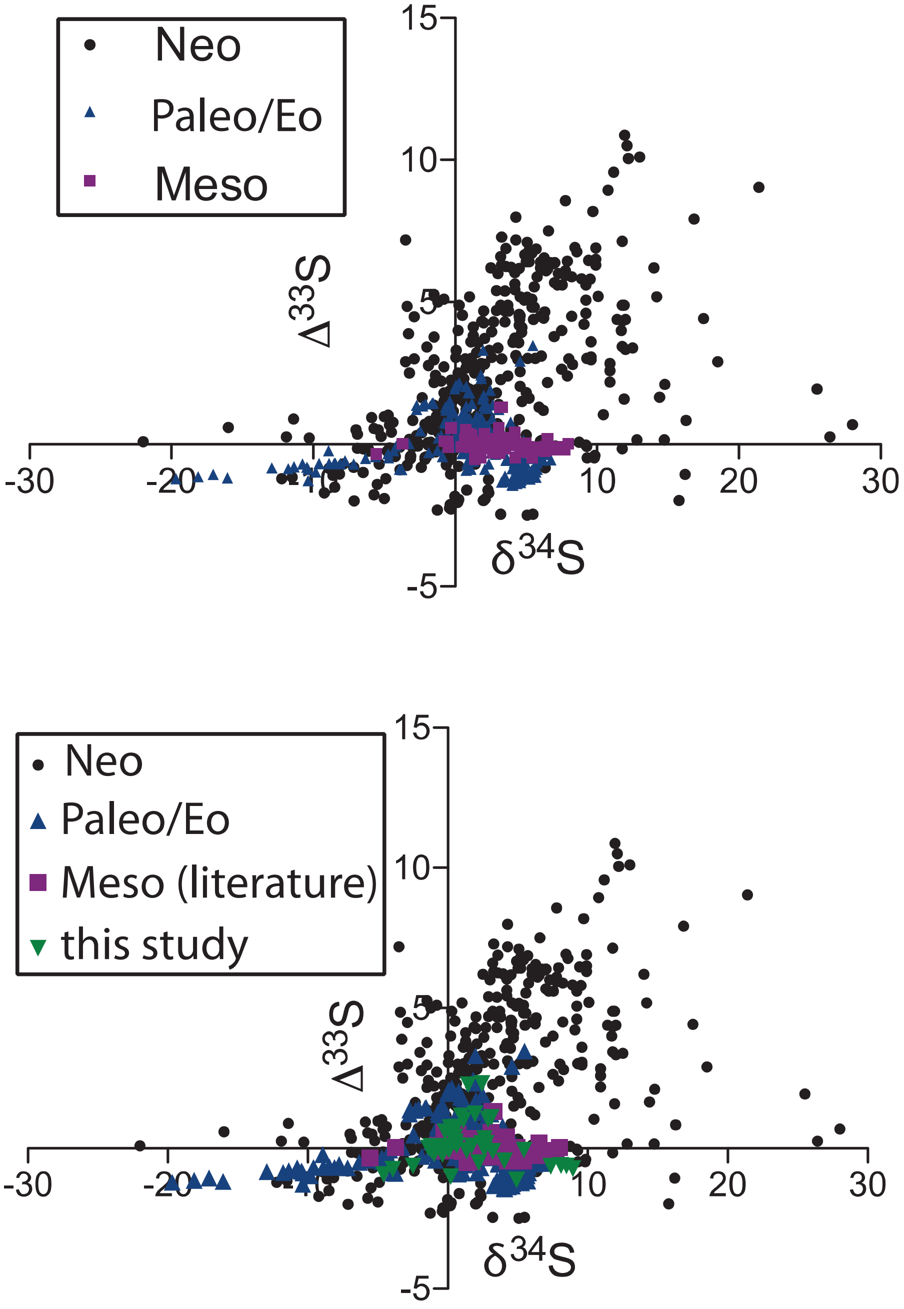

Figure 2.11: Literature data includes only bulk extractions. Compared to the previous Mesoarchaean samples our dataset follows more similar to Paleo and Neoarchaean systematics showing the diagonal distribution attributed to atmospheric contributions and horizontal variations attributed to microbial processing.

Changes in volcanism is a possible mechanism for diluting atmospheric S-MIF without changing S-MIF production or preservation. Changes in the redox state of volcanic flux has been linked to a trigger mechanism for atmosphere oxidation (Kasting et al., 1993). Kasting et al, propose that loss of atmospheric H_2 would increase atmospheric and mantle O_2. Increases the oxygen fugacity changes the oxidation state of sulfur (Fincham and Richardson, 1954; Jugo et al., 2005). Additionally, sulfur content is less at lower oxygen fugacities (Jugo et al., 2010). The variation of SO_2 to H_2S in volcanic sulfur input has implication for the S-MIF record. H_2S does not undergo photodissociation so by increasing the atmospheric input of H_2S the S-MIF reservoir in the atmosphere is diluted (Halevy et al., 2010). Increasing the input of H_2S to the atmosphere augments the amount of reduced sulfur with a $\Delta^{33}S \approx 0$. Mixing with the reduced sulfur pool from SO_2 photodissociation causes a diminishment of positive $\Delta^{33}S$. Ono and coworkers, through modeling, found that the amount of S_8 deposited out of total sulfur is strongly dependent on total sulfur outgassing (Ono et al., 2003). In addition, the production rate of S_8 is inversely proportional to average $\Delta^{33}S$. As the production rate of S_8 increases, the average $\Delta^{33}S$ decreases(Ono et al., 2003). S_8 carries a positive $\Delta^{33}S$ so volcanic sulfur outputs could have implications for the magnitude of the positive $\Delta^{33}S$. A greater flux of volcanoes would have the effect of diminishing positive $\Delta^{33}S$. The methane haze hypothesis would cause a decrease in negative $\Delta^{33}S$. A high-altitude methane haze blocking some of the ultraviolet rays necessary for photodissociation of SO_2 causes an oxidized sulfur pool with $\Delta^{33}S \approx 0$. The non-MIF sulfur dilutes the oxidized sulfur carrying a negative $\Delta^{33}S$.

Our measurements indicate a larger spread within the Mesoarchaean data. The consistency with the Archaean reference array and more similar magnitude between Eo, Paleo and Mesoarchaean samples indicates similar processes controlling mass independent fractionation between these times frames. The most pressing question in mass independent sulfur isotopes in the Archaean is no longer why are the values so low within the Mesoarchaean, as they are in fact more similar to older Archaean results, but rather what caused the blossoming of $\Delta^{33}S$ ranges within the Neoarchaean. There is a drastic explosion in range both in positive $\Delta^{33}S$ and negative $\Delta^{33}S$ during the Neoarchaean.

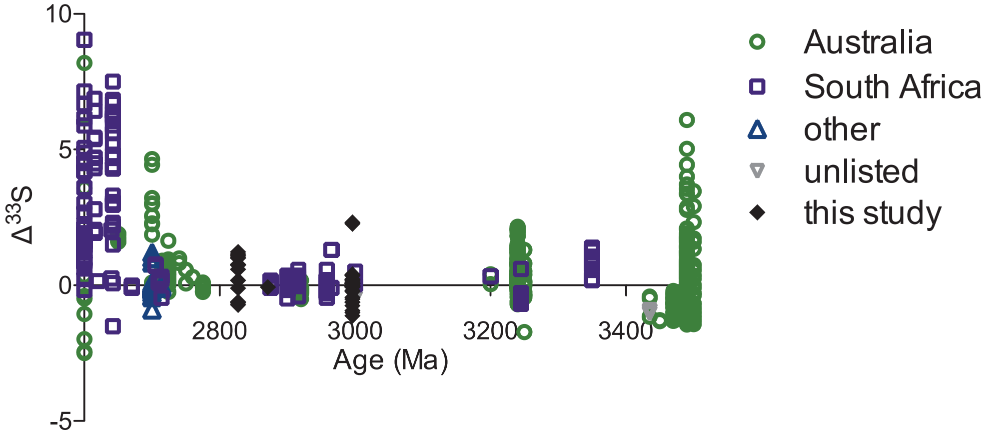

Figure 2.12: Updated location distribution. A new sample set has been added to the Mesoarchaean. This sample set expands the geographic range of samples in the Mesoarchaean while also looking at lithologic relationships.

An intriguing observation involves the pillow basalt chill margins. In this study, we measured pillow basalt chill margins and interior pillows which yield results similar to model estimates for seawater sulfate. Mantle sulfur has a $\delta^{34}S \approx 0 \pm 2‰$ $\Delta^{33}S \approx 0.00 \pm 0.03‰$ (Farquhar et al., 2002; Seal II, 2006). Ono et al. estimate Archaean seawater sulfate to range from $\delta^{34}S$ = 6-16‰ with a $\Delta^{33}S \approx -2‰$ (Ono et al., 2003). Our $\delta^{34}S$ values fall within the range proposed by Ono et al, at 7.36 to 8.94‰; however, our $\Delta^{33}S$ are smaller but still negative ranging from -0.61 to -0.72‰. Negative $\Delta^{33}S$ values are consistent with Archaean barites (Farquhar et al., 2000a). A sulfide-rich shale from Red Lake carries a very similar $\delta^{34}S$ and $\Delta^{33}S$ to the measured pillow basalts. Although this study does not have substantial evidence to fully support the notion, it would be interesting to further investigate the potential of chill margins as a proxy for Archaean seawater sulfate isotope ratios.

Evidently, lithology impacts the sulfur isotope signal. Samples which carry positive $\Delta^{33}S$ include shales, volcanoclastic, and BIF whereas negative $\Delta^{33}S$ are recorded in pillow basalts, pyrite nodules, and cherts. Carbonates and concentrated sulfide deposits have both positive and negative $\Delta^{33}S$. The largest magnitudes are recorded in concentrated sulfide deposits.

Certain difference may be caused by the difference in sampling the entire water column as opposed to a more instantaneous sample of a smaller water volume. The difference in cherty component seems to influence S-MIF as well. The $\Delta^{33}S$ magnitude in the silica-rich layer is double compared to the silica-poor layer. The difference in the cherty component of the sediments could relate to deposition duration and hence the amount of input from atmosphere.

Conclusion

Our data from Northwestern Ontario greenstone belts increases the magnitude of Mesoarchaean MIF from the previously published data.. The Mesoarchaean minimum does not seem quite so drastic. Rather than a significantly decreased Mesoarchaean S-MIF, the Mesoarchaean seems to have a range more similar to the Paleo and Eoarchaean. In addition, the $\Delta^{33}S$ versus $\Delta^{36}S$ plot has a slope of -1 which is similar to the rest of the Archaean data. Since the slope is consistent with the other Archaean slopes, this may indicate that similar photochemistry was taking place but during the Mesoarchaean dilution occurred.

Furthermore, there is a lithologic control on S-MIF. Chemically and biologically precipitated sulfides contain MIF whereas clastic rocks have S-MIF ≈ 0. Pillow basalts may provide a proxy for seawater sulfate. The relatively large positive $\delta^{34}S$ and negative $\Delta^{33}S$ could not be derived from source volcanic material and must result from interaction with a source which carries atmospheric S-MIF. The S-MIF pool could be the Archaean ocean.

The drastic change in the magnitude of S-MIF occurs in the Neoarchaean. Possibilities for this change include a reduction in dilution mechanisms which are dampening the MIF effect in older Archaean samples such as a change in style of volcanism where more SO_2 rather than H_2S are being sourced into the Archaean atmosphere.

Works Cited

Bao, H.M., Rumble, D., Lowe, D.R., 2007. The five stable isotope compositions of Fig Tree barites: Implications on sulfur cycle in ca. 3.2 Ga oceans. Geochimica Et Cosmochimica Acta 71, 4868-4879.

Baublys, K., Golding, S., Young, E., Kamber, B., 2004. Simultaneous determination of delta (33) SV-CDT and delta S-34(V-CDT) using masses 48, 49 and 50 on a continuous flow isotope ratio mass spectrometer. Rapid Communications in Mass Spectrometry 18, 2765-2769.

Bekker, A., Holland, H.D., Wang, P.L., Rumble, D., Stein, H.J., Hannah, J.L., Coetzee, L.L., Beukes, N.J., 2004. Dating the rise of atmospheric oxygen. Nature 427, 117-120.

Buse, S., Lewis, D., Magnus, S., 2009. Field investigations in the Lumby Lake greenstone belt, NW Ontario: New insights into the geology, structure and economic potential; *in* Summary of Field Work and Other Activities 2009, Ontario Geological Survey, pp. 15-11 to 15-15.

Buse, S., Lewis, D., Magnus, S., 2010. Precambrian geology of the Lumby Lake greenstone belt, Ontario Geological Survey.

Canfield, D.E., Raiswell, R., Westrich, J.T., Reaves, C.M., Berner, R.A., 1986. The use of chromium reduction in the analysis of reduced inorganic sulfurin sediments and shales. Chemical Geology 54, 149-155.

Cates, N.L., Mojzsis, S.J., 2006. Chemical and isotopic evidence for widespread Eoarchean metasedimentary enclaves in southern West Greenland. Geochimica Et Cosmochimica Acta 70, 4229-4257.

Cheney, E., 1996. Sequence stratigraphy and plate tectonic significance of the Transvaal succession of southern Africa and its equivalent in Western Australia. Precambrian Research 79, 3-24.

Cloud, P., 1972. Working model of primitive Earth. American Journal of Science 272, 537-548.

Cloud, P., 1973. Paleoecological significance of banded iron formation. Economic Geology 68, 1135-1143.

Corfu, F., Andrews, A., 1987. Geochronological constraints on the timing of magmatism, deformation, and gold mineralization in the Red Lake Greesntone-Belt, Northwestern Ontario. Canadian Journal of Earth Sciences 24, 1302-1320.

Corfu, F., Davis, D., Stone, D., Moore, M., 1998. Chronostratigraphic constraints on the genesis of Archean greenstone belts, northwestern Superior Province, Ontario, Canada. Precambrian Research 92, 277-295.

Corfu, F., Stott, G., 1993. Age and petrogenesis of 2 late Archean magmatic suites, Northwestern Superior Province, Canada - Zircon U-Pb and Lu-Hf Isotopic Relations. Journal of Petrology 34, 817-838.

Corfu, F., Wallace, H., 1986. U-Pb zircon ages for magmatism in the Red Lake Greenstone-Belt, Northwestern Ontario. Canadian Journal of Earth Sciences 23, 27-42.

Davis, D., Jackson, M., 1988. Geochronology of the Lumby Lake Greenstone-Belt - A 3-Ga complex within the Wabigoon Subprovince, Northwest Ontario. Geological Society of America Bulletin 100, 818-824.

de Kock, M., Beukes, N., Armstrong, R., 2012. New SHRIMP U-Pb zircon ages from the Hartswater Group, South Africa: Implications for correlations of the Neoarchean

Ventersdorp Supergroup on the Kaapvaal craton and with the Fortescue Group on the Pilbara craton. Precambrian Research 204, 66-74.

de Kock, M., Evans, D., Beukes, N., 2009. Validating the existence of Vaalbara in the Neoarchean. Precambrian Research 174, 145-154.

Ding, T., Valkiers, S., Kipphardt, H., De Bievre, P., Taylor, P., Gonfiantini, R., Krouse, R., 2001. Calibrated sulfur isotope abundance ratios of three IAEA sulfur isotope reference materials and V-CDT with a reassessment of the atomic weight of sulfur. Geochimica Et Cosmochimica Acta 65, 2433-2437.

Domagal-Goldman, S.D., Kasting, J.F., Johnston, D.T., Farquhar, J., 2008. Organic haze, glaciations and multiple sulfur isotopes in the Mid-Archean Era. Earth and Planetary Science Letters 269, 29-40.

Farquhar, J., Bao, H.M., Thiemens, M., 2000a. Atmospheric influence of Earth's earliest sulfur cycle. Science 289, 756-758.

Farquhar, J., Peters, M., Johnston, D.T., Strauss, H., Masterson, A., Wiechert, U., Kaufman, A.J., 2007. Isotopic evidence for Mesoarchaean anoxia and changing atmospheric sulphur chemistry. Nature 449, 706-709.

Farquhar, J., Savarino, J., Airieau, S., Thiemens, M.H., 2001. Observation of wavelength-sensitive mass-independent sulfur isotope effects during SO2 photolysis: Implications for the early atmosphere. Journal of Geophysical Research-Planets 106, 32829-32839.

Farquhar, J., Savarino, J., Jackson, T.L., Thiemens, M.H., 2000b. Evidence of atmospheric sulphur in the martian regolith from sulphur isotopes in meteorites. Nature 404, 50-52.

Farquhar, J., Wing, B., 2003. Multiple sulfur isotopes and the evolution of the atmosphere. Earth and Planetary Science Letters 213, 1-13.

Farquhar, J., Wing, B., McKeegan, K., Harris, J., Cartigny, P., Thiemens, M., 2002. Mass-independent sulfur of inclusions in diamond and sulfur recycling on early earth. Science 298, 2369-2372.

Fenwick, K., 1976. Geology of the Finlayson Lake area, District of Rainy River, in: Mines, O.D.o. (Ed.). Geosciences Report, Toronto, p. 86.

Fincham, C., Richardson, F., 1954. The behaviour of sulphur in silicate and aluminate melts. Proceedings of the Royal Society of London Series a-Mathematical and Physical Sciences 223, 40-62.

Fralick, P., Hollings, P., King, D., Condie, K., V, P., 2008. Stratigraphy, geochemistry, and depositional environments of Mesoarchean sedimentary units in western Superior Province: Implications for generation of early crust. When Did Plate Tectonics Begin on Planet Earth 440, 77-96.

Golding, S.D., Duck, L.J., Young, E., Baublys, K.A., Glikson, M., Kamber, B.S., 2011. Earliest Seafloor Hydrothermal Systems on Earth: Comparison with Modern Analogues. Springer.

Guo, Q.J., Strauss, H., Kaufman, A.J., Schroder, S., Gutzmer, J., Wing, B., Baker, M.A., Bekker, A., Jin, Q.S., Kim, S.T., Farquhar, J., 2009. Reconstructing Earth's surface oxidation across the Archean-Proterozoic transition. Geology 37, 399-402.

Halevy, I., Johnston, D.T., Schrag, D.P., 2010. Explaining the Structure of the Archean Mass-Independent Sulfur Isotope Record. Science 329, 204-207.

Hoffman, P., 1988. United plates of America, the birth of a craton - early Proterozoic assembly and growth of Laurentia. Annual Review of Earth and Planetary Sciences 16, 543-603.

Hofmann, H., Thurston, P., Wallace, H., 1985. Archean stromatolites from Uchi greenstone belt, northwestern Ontario. Geological Association of Canada, St. Johns, Canada.

Hou, K.J., Li, Y.H., Wan, D.F., 2007. Constraints on the Archean atmospheric oxygen and sulfur cycle from mass-independent sulfur records from Anshan-Benxi BiFs., Liaoning Province, China. Science in China Series D-Earth Sciences 50, 1471-1478.

Hu, G., Rumble, D., Wang, P., 2003. An ultraviolet laser microprobe for the in situ analysis of multisulfur isotopes and its use in measuring Archean sulfur isotope mass-independent anomalies. Geochimica Et Cosmochimica Acta 67, 3101-3118.

Jamieson, J.W., Wang, B.A., Hannington, M.D., Farquhar, J., 2006. Evaluating isotopic equilibrium among sulfide mineral pairs in Archean ore deposits: Case study from the Kidd Creek VMS deposit, Ontario, Canada. Economic Geology 101, 1055-1061.

Johnston, D.T., Farquhar, J., Summons, R.E., Shen, Y., Kaufman, A.J., Masterson, A.L., Canfield, D.E., 2008. Sulfur isotope biogeochemistry of the Proterozoic McArthur Basin. Geochimica Et Cosmochimica Acta 72, 4278-4290.

Johnston, D.T., Poulton, S.W., Fralick, P.W., Wing, B.A., Canfield, D.E., Farquhar, J., 2006. Evolution of the oceanic sulfur cycle at the end of the Paleoproterozoic. Geochimica Et Cosmochimica Acta 70, 5723-5739.

Johnston, D.T., Wing, B.A., Farquhar, J., Kaufman, A.J., Strauss, H., Lyons, T.W., Kah, L.C., Canfield, D.E., 2005. Active microbial sulfur disproportionation in the Mesoproterozoic. Science 310, 1477-1479.

Jugo, P., Luth, R., Richards, J., 2005. Experimental data on the speciation of sulfur as a function of oxygen fugacity in basaltic melts. Geochimica Et Cosmochimica Acta 69, 497-503.

Jugo, P., Wilke, M., Botcharnikov, R., 2010. Sulfur K-edge XANES analysis of natural and synthetic basaltic glasses: Implications for S speciation and S content as function of oxygen fugacity. Geochimica Et Cosmochimica Acta 74, 5926-5938.

Kasting, J., Eggler, D., Raeburn, S., 1993. Mantle redox evolution and the oxidation-state of the Archean atmosphere. Journal of Geology 101, 245-257.

Kasting, J., Zahnle, K., Pinto, J., Young, A., 1989. Sulfur, ultraviolet-radiation, and the early evolution of life. Origins of Life and Evolution of the Biosphere 19, 95-108.

Kaufman, A.J., Johnston, D.T., Farquhar, J., Masterson, A.L., Lyons, T.W., Bates, S., Anbar, A.D., Arnold, G.L., Garvin, J., Buick, R., 2007. Late Archean biospheric oxygenation and atmospheric evolution. Science 317, 1900-1903.

King, D., 1998. Depositional environments of the 3.0 Ga Finlayson and Lumby Lake Greenstone belts, Superior Province, Ontario, Geology. Lakehead University, Thunder Bay, Ontario.

Mojzsis, S., Coath, C., Greenwood, J., McKeegan, K., Harrison, T., 2003. Mass-independent isotope effects in Archean (2.5 to 3.8 Ga) sedimentary sulfides determined by ion microprobe analysis. Geochimica Et Cosmochimica Acta 67, 1635-1658.

Nunes, P., Thurston, P., 1980. 220 million years of Archean evolution - a zircon U-Pb age stratigraphic study of the Uchi-Confederation lakes greenstone-belt, northwester Ontario. Canadian Journal of Earth Sciences 17, 710-721.

Ohmoto, H., Watanabe, Y., Ikemi, H., Poulson, S.R., Taylor, B.E., 2006. Sulphur isotope evidence for an oxic Archaean atmosphere. Nature 442, 908-911.

Ono, S., Beukes, N.J., Rumble, D., Fogel, M.L., 2006a. Early evolution of atmospheric oxygen from multiple-sulfur and carbon isotope records of the 2.9 Ga Mozaan Group of the Pongola Supergroup, Southern Africa. South African Journal of Geology 109, 97-108.

Ono, S., Eigenbrode, J., Pavlov, A., Kharecha, P., Rumble, D., Kasting, J., Freeman, K., 2003. New insights into Archean sulfur cycle from mass-independent sulfur isotope records from the Hamersley Basin, Australia. Earth and Planetary Science Letters 213, 15-30.

Ono, S., Wing, B., Johnston, D., Farquhar, J., Rumble, D., 2006b. Mass-dependent fractionation of quadruple stable sulfur isotope system as a new tracer of sulfur biogeochemical cycles. Geochimica Et Cosmochimica Acta 70, 2238-2252.

Ono, S.H., Beukes, N.J., Rumble, D., 2009a. Origin of two distinct multiple-sulfur isotope compositions of pyrite in the 2.5 Ga Klein Naute Formation, Griqualand West Basin, South Africa. Precambrian Research 169, 48-57.

Ono, S.H., Kaufman, A.J., Farquhar, J., Sumner, D.Y., Beukes, N.J., 2009b. Lithofacies control on multiple-sulfur isotope records and Neoarchean sulfur cycles. Precambrian Research 169, 58-67.

Papineau, D., Mojzsis, S., 2006. Mass-independent fractionation of sulfur isotopes in sulfides from the pre-3770 Ma Isua Supracrustal Belt, West Greenland. Geobiology 4, 227-238.

Papineau, D., Mojzsis, S.J., Schmitt, A.K., 2007. Multiple sulfur isotopes from Paleoproterozoic Huronian interglacial sediments and the rise of atmospheric oxygen. Earth and Planetary Science Letters 255, 188-212.

Partridge, M., Golding, S., Baublys, K., Young, E., 2008. Pyrite paragenesis and multiple sulfur isotope distribution in late Archean and early Paleoproterozoic Hamersley Basin sediments. Earth and Planetary Science Letters 272, 41-49.

Pavlov, A.A., Kasting, J.F., 2002. Mass-independent fractionation of sulfur isotopes in Archean sediments: Strong evidence for an anoxic Archean atmosphere. Astrobiology 2, 27-41.

Philippot, P., Van Zuilen, M., Lepot, K., Thomazo, C., Farquhar, J., Van Kranendonk, M., 2007. Early Archaean microorganisms preferred elemental sulfur, not sulfate. Science 317, 1534-1537.

Rogers, N., 2002. Geology, Confederation Lake, Ontario scale 1:50 000, in: Geological Survey of Canada. Ottawa, Ontario, Canada.

Rouxel, O., Ono, S.H., Alt, J., Rumble, D., Ludden, J., 2008. Sulfur isotope evidence for microbial sulfate reduction in altered oceanic basalts at ODP Site 801. Earth and Planetary Science Letters 268, 110-123.

Sanborn-Barrie, M., Skulski, T., Parker, J., 2001. Three hundred million years of tectonic history recorded by the Red Lake greenstone belt, Ontario; Current Research 2001-C19, in: Geological Survey of Canada , p. 19.

Schroder, S., Lacassie, J., Beukes, N., 2006. Stratigraphic and geochemical framework of the Agouron drill cores, Transvaal Supergroup (Neoarchean-Paleoproterozoic, South Africa). South African Journal of Geology 109, 23-54.

Seal II, R.R., 2006. Sulfur Isotope Geochemistry of Sulfide Minerals. Reviews in Mineralogy and Geochemistry, pp. 633-677.

Shen, Y.N., Farquhar, J., Masterson, A., Kaufman, A.J., Buick, R., 2009. Evaluating the role of microbial sulfate reduction in the early Archean using quadruple isotope systematics. Earth and Planetary Science Letters 279, 383-391.

Stone, D., 2008. Precambrian geology, Atikokan area, in: Ontario Geological Survey.

Stone, D., Pufhal, P., 1995. Geology of the Atikokan-Sapawe area: regional controls on gold mineralization in the Marmion batholith, in: Summary of Field Work and Other Activities, Ontario Geological Survey pp. 45-57.

Stott, G.M., Corkery, M.T., Percival, J.A., Simard, M., Goutier, J., 2010. A revised terrane subdivision of the Superior Province, *in* Summary of Field Work and Other Activities. Ontario Geological Survey, pp. 20-21 - 20-10.

Thomazo, C., Ader, M., Farquhar, J., Philippot, P., 2009. Methanotrophs regulated atmospheric sulfur isotope anomalies during the Mesoarchean (Tumbiana Formation, Western Australia). Earth and Planetary Science Letters 279, 65-75.

Tomlinson, K., Davis, D., Stone, D., Hart, T., 2003. U-Pb age and Nd isotopic evidence for Archean terrane development and crustal recycling in the south-central Wabigoon subprovince, Canada. Contributions To Mineralogy and Petrology 144, 684-702.

Tomlinson, K., Stevenson, R., Hughes, D., Hall, R., Thurston, P., Henry, P., 1998. The Red Lake greenstone belt, Superior Province: evidence of plume-related magmatism at 3 Ga and evidence of an older enriched source. Precambrian Research 89, 59-76.

Ueno, Y., Ono, S., Rumble, D., Maruyama, S., 2008. Quadruple sulfur isotope analysis of ca. 3.5 Ga Dresser Formation: New evidence for microbial sulfate reduction in the early Archean. Geochimica Et Cosmochimica Acta 72, 5675-5691.

Whitehouse, M.J., Kamber, B.S., Fedo, C.M., Lepland, A., 2005. Integrated Pb- and S-isotope investigation of sulphide minerals from the early Archaean of southwest Greenland. Chemical Geology 222, 112-131.

Williford, K., Van Kranendonk, M., Ushikubo, T., Kozdon, R., Valley, J., 2011. Constraining atmospheric oxygen and seawater sulfate concentrations during Paleoproterozoic glaciation: In situ sulfur three-isotope microanalysis of pyrite from the Turee Creek Group, Western Australia. Geochimica Et Cosmochimica Acta 75, 5686-5705.

Zegers, T., de Wit, M., Dann, J., White, S., 1998. Vaalbara, Earth's oldest assembled continent? A combined structural, geochronological, and palaeomagnetic test. Terra Nova 10, 250-259.

Zerkle, A., Claire, M., Domagal-Goldman, S., Farquhar, J., Poulton, S., 2012. A bistable organic-rich atmosphere on the Neoarchaean Earth. Nature Geoscience 5, 359-363.

Concluding remarks

Multiple sulfur isotopes are a powerful tool to learn about biogeochemistry. Throughout this thesis both the mass dependent and the mass independent systematics of sulfur isotopes are explored. Both sample localities are located within in Canada.

With regards to sulfur oxidation, large fractionation have been measured which is contrary to the current sulfur oxidation paradigm. There may be systematics at low temperatures which are causing these unusual fractionations. Understanding the reactions resulting in these fractionations could be crucial in future interpretations involving sulfur isotopes in oxidizing systems such as the surface of Mars. With the potential for measuring sulfur isotopes on the newest rover, Curiosity, interpretation of sulfur isotopes should be mindful of various processes which can cause fractionation in an oxidizing environment.

For Mesoarchaean geology, the range of the sulfur isotope dataset has been expanded within the Mesoarchaean and an additional locality has been added to the previous dataset, which only included samples from Australia and South Africa. Although the Mesoarchaean Δ^{33}S magnitude is still small compared to adjoining time periods, the sulfur isotope systematics appear much more similar than previously thought. Our Mesoarchaean samples follow the Archaean reference array, albeit with a diminished range. In addition, in this dataset the isotope systematics of Δ^{33}S versus Δ^{36}S displays the Archaean slope of -1.